

# Performance of dense wireless networks in 5G and beyond using stochastic geometry

*Reza Aghazadeh(\*) and Umberto Spagnolini*

*{Reza.Aghazadeh@polimi.it; Umberto.Spagnolini@polimi.it}*

Dep. Elettronica, Informazione and Bioingegneria, Politecnico di Milano, Milan (Italy) (\*)  
corresponding author

## Abstract

Device density in cellular networks is expected to increase considerably in the next future. Accordingly, the access point (AP) will equip massive multiple-input multiple-output (mMIMO) antennas, using collimated millimeter-wave (mmW) and sub-THz communications, and increase the bandwidth to accommodate the growing data rate demands. In this scenario, interference plays a critical role and, if not characterized and mitigated properly, might limit the performances of the network. In this context, this paper derives the statistical properties of the aggregated interference power for a cellular network equipping a mMIMO cylindrical array. The proposed statistical model considers the link blockage and other network parameters such as antenna configuration and device density. The findings show that the characteristic function (CF) of the aggregated interference power can be regarded as a weighted mixture of two alpha-stable distributions. Furthermore, by analyzing the service probability, it is found that there is an optimal configuration of the array depending on the AP height and device density. The proposed statistical model can be part of the design of dense networks providing valuable insights for optimal network deployment.

**Keywords:** 5G- mmW, 6G systems, Poisson point process, Interference characterization, Stochastic geometry, Outage analysis, Beamforming, Uplink, Uniform cylindrical array, Blockage

## I. INTRODUCTION

The fifth-generation (5G) cellular network has been recently deployed with unprecedented communication performance, i.e., 10-100X times higher data rate, 1ms latency, and much higher area throughput [1], [2]. The upcoming sixth-generation (6G) cellular network promises to further improve current performance by at least one order of magnitude [3]. To meet such

requirements, it is necessary to operate on multiple frontiers, e.g., increase the bandwidth, cell density, transceiver efficiency.

Current cellular networks operate at sub-6GHz band, which is heavily congested [3]. Recently millimeter waves (mmW) and sub-THz frequencies (30 – 300GHz) have gained a substantial interest because of the large unexploited spectrum [4]–[6]. However, propagation at these frequencies experiences higher path and penetration loss making the links prone to blockage [7]. A solution to these challenges is to use beam-type communication based on massive multiple-input multiple-output (mMIMO) systems and increase cell density [8]. However, as the device density increases, interference emerges as one of the main challenges to be characterized and mitigated. Characterization of the aggregate interference power and coverage analysis in millimeter-wave (mmW) networks has been investigated over the past years but only in some specialized settings, under the line-of-sight (LOS) and non-line-of-sight (NLOS) propagation. Win et. al. [9] derived the distribution of the aggregate interference power and amplitude for PPP distributed user equipments (UEs) on a 2D plane when the antenna is omnidirectional and co-planar with UEs (array's height  $h = 0$ ). The impact analysis of the users' height has been studied in ref. [10]. The array's height  $h$  plays an important role that needs to be analyzed, namely in view of the 5G mmW and 6G use-cases. Therefore, it is necessary to extend the Stochastic Geometry (SG) framework to the 3D framework of antennas and UEs (see e.g. [11]). SG provides a preferred framework in network modeling to perform coverage and rate performance analysis [12]–[16]. The impact of the antennas' height in a 3D SG for ultra-dense networks proves that there is an upper limit on network performance which is dependent on the path-loss model parameters [17]. Even if the impact of the antenna and user equipment (UE) height difference has been studied [18], the existence of an optimum array height has not been deduced in dense networks. Here we derive the analytical model of aggregated interference and show that the optimum array height depends on the path-loss model but also on the users' density, array type, and size. Similarly, the impact of the height in low-altitude aerial platforms [19], [20] and in unmanned aerial vehicles [21], [22] proves that there are optimum altitudes maximizing the coverage probability according to some specific scenarios. In the literature, it is common to assume that the fading follows Rayleigh distribution (or at least the interference link has a Rayleigh distribution) or Nakagami- $m$  distribution. The coverage probability has a tractable form as a Laplace function of the aggregate interference power (see, e.g. [12], [23]–[25]). However, for general fading, using the Laplace function of the aggregate interference is not possible anymore and thus, the coverage and rate analysis cannot be expressed in a tractable way. To

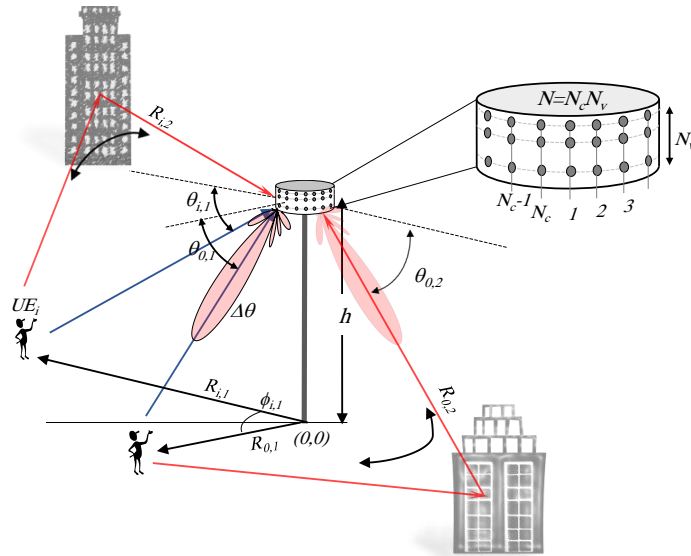


Figure 1. Configuration of a  $N_c \times N_v$  uniform cylindrical array (UcylA) with line-of-sight (LOS) and non-line-of-sight (NLOS) links:  $(\phi_{i,\ell}, \theta_{i,\ell})$  are the azimuth and elevation angles,  $h$  is the height of the array and the pointing directions are toward all the LOS ( $\ell = 1$ ) and NLOS ( $\ell = 2, 3, \dots$ ) links arriving from the user equipment (UE) over a propagation path  $R_{i,\ell}$ .

overcome this problem, ref. [13] introduces multiple techniques, including some methods to find the probability density function (PDF) of the aggregate interference calculated from the corresponding characteristic function (CF).

In previous works, interference distribution for single antennas or the uniform linear array (ULA) (e.g. in [23]), configuration were investigated most. The contribution of this paper is the usage of the 3D SG framework in the uplink for homogeneous Poisson point process (PPP) with a density  $\lambda$  on a pseudo-3D geometry (sometimes referred to as 2.5D geometry [26], [27]) where UEs lie in a plane (say ground) and the access point (AP) with  $N_c \times N_v$  uniform cylindrical array (UcylA) (i.e. a set of  $N_v$  half-wavelength rings of  $N_c$  uniform circular array (UCA) antennas/each) has the height  $h \geq 0$ . The Fig. 1 illustrates the setup for the computation of the properties of the aggregate interference from the ensemble of  $UE_1, UE_2, \dots, UE_i, \dots$  when the array at the AP is pointing toward the user of interest  $UE_0$ . We show that being able to characterize the aggregated interference, one can optimally adjust the configurations of the AP to increase the number of users served and accordingly the coverage probability.

We analytically prove in Sect.IV that the aggregated interference power onto an array of antennas located in an arbitrary height ( $h$ ) has a CF that can be decomposed into a mixture of

two stable distributions (a skewed alpha-stable and a Gaussian distribution). The closed-form CF for  $h > 0$  is another novelty to compute the PDF or cumulative density function (CDF) of the aggregated interference power, without cumbersome numerical integration. The scenario considered herein for users and interferers accounts either the LOS and NLOS propagation, and also the possibility of link blockage as typical in mmW and sub-THz systems. The analytical model enables (Sect.III-D) the evaluation of the trade-off in arrays' height selection, and the impact of the propagation scenarios. The UcyLA with  $h > 0$  generalizes the previous works on ULA configuration that was investigated mostly for coverage analysis (see, e.g., [23], [28]). On array engineering, UcyLA can be designed by multifaceted array as far more practical, and results in [29] supports the conclusion that any results for curved arrays apply to faceted ones.

Based on the analytical model, the main results can be summarized as follow: i) in most scenarios with small interferers' density it is more beneficial to adopt a UCA rather than UcyLA while for large interferers' density a UcyLA would be preferred; ii) there is an optimum AP height that depends on propagation and interferers' density  $\lambda$ ; iii) at AP height  $h = 0$  the aggregated interference power is alpha-stable distributed, and for  $h \rightarrow \infty$  the limit becomes Gaussian, but for any arbitrary height  $h$  it is decomposable into two stable distributions; iv) blockage probability is impacting the service probability for small  $\lambda$ , but less if counting the average number of users served within a region; v) a connection with multiple paths (LOS and NLOS) is more beneficial for small  $\lambda$ , as for large  $\lambda$  the interference is too large.

The paper is organized as follows. We present the system model including the signal and array gain models in Sect.II. The CF of the aggregate interference for UcyLA in LOS links in Sect.III. Sect IV contains the statistical characterization of the interference power. In Sect.V the CF is extended considering NLOS paths, noise power and blockage, and we conclude the paper in Sect.VI.

## II. SYSTEM MODEL

The scenario is in Fig. 1 where the AP has a cylindrical array with  $N = N_c \times N_v$  antennas in total. The UEs are uniformly distributed following a homogeneous PPP with density  $\lambda$  that denotes the mean number of active UEs per square meter. The spatial channel of the mmW and 6G sub-THz systems are purely directional (see, e.g., [30]), and the LOS (or NLOS) link is affected by the path-loss modeled in terms of UE-AP distance  $d_{LOS}$  (or  $d_{NLOS}$ ), and faded amplitude  $\beta_{LOS}$  (or  $\beta_{NLOS}$ ). The propagation attenuation model for LOS and NLOS is  $\beta/d^b$  with amplitude path-loss  $b \geq 1$ . The array of antennas is uniformly cylindrical, the

isotropic radiating antennas are arranged into a set of  $N_v$  UCAs with  $N_c$  antennas each and antennas' spacing is half the wavelength. Namely, the two arrangements of antennas are such that the corresponding beamforming of UCAs reduce the interference angularly, and the vertical arrangement of the rings (acting as vertical ULAs), tilts the beam to improve the capability to reduce the near interferers when pointing toward far-away UEs. Note that here the UEs are considered on the ground, which means that the AP height is the height difference of UEs and AP (pseudo 3D or 2.5D geometry).

#### A. Array gain model

Each AP equipped with the array of antennas is positioned at height  $h$  from the ground at  $(0, 0)$  planar coordinates as in Fig. 1. The array gain for the UcyLA in far-field  $G(\phi, \theta)$  depends on elevation angle ( $\theta$ ) and azimuth ( $\phi$ ), which in turn depends on the number of antennas partitioning between  $N_v$  and  $N_c$ . The beamforming for the cylindrical array is conveniently decomposed into the design of two compound arrays, and thus the array gain  $G(\phi, \theta) = G_c(\phi)G_v(\theta)$  is separable into the UCA gain  $G_c(\phi)$  and vertical ULA gain  $G_v(\theta)$  [31], [32]. The approximation holds true in UcyLA when using separable weightings [33], [34]. The beamforming used here is the conventional one that is optimum for uniform interference, and the array gains for half-wavelength inter-element spacing either for UCA and ULA are [34], [35]:

$$G_c(\phi) = J_0 \left( \frac{N_c}{2} \sqrt{(\cos \phi - \cos \phi_o)^2 + (\sin \phi - \sin \phi_o)^2} \right) \quad (1)$$

$$G_v(\theta) = \frac{\sin[\pi(\sin \theta - \sin \theta_o)N_v/2]}{N_v \sin[\pi(\sin \theta - \sin \theta_o)/2]} \quad (2)$$

where  $(\phi_o, \theta_o)$  denotes the pointing azimuth and elevation pair to the intended UE, and for UCA the gain approximation 1 is by the zero-order Bessel function of the first kind  $J_0(\cdot)$  that can be shown to be accurate for  $N_c \geq 16$ . Note that array gains are normalized for convenience to have  $G(\phi_o, \theta_o) = 1$ . The beam width along the two angles,  $\Delta\phi$ , and  $\Delta\theta$ , are inversely proportional to  $N_c$  and  $N_v$ , respectively. Elevation beam width is further distorted by the effective array aperture that makes the beam width scale with the cosine of the tilt angle (stretching effect):  $\Delta\theta/\cos(\theta - \theta_o)$ .

#### B. Signal model and service probability

Let  $x$  be the transmitted signal, the signal received by the AP with beamforming pointing toward the UE of interest with angles  $\phi_o = 0$  and radial distance  $R_o$  is

$$y = \frac{\beta_o}{(R_o^2 + h^2)^{\frac{b}{2}}} G(\phi_o, \theta_o)x + \iota + w, \quad (3)$$

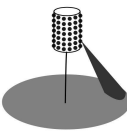
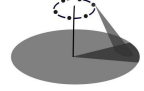

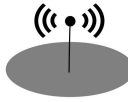

	UcylA	UCA $h > 0$	UCA $h = 0$	Isotropic $h > 0$	Isotropic $h = 0$
					
$N_c$	$>1$	$>1$	$>1$	1	1
$N_v$	$>1$	1	1	1	1
$h$	$\geq 0$	$\geq 0$	0	$\geq 0$	0
	Sect.III-A CF: (14)	Sect.III-B CF: (18)	Sect.III-B CF: (22)	Sect.III-B CF: (24)	Ref [9]

Table I

ARRAY CONFIGURATIONS AND REFERENCE TO THE CHARACTERISTIC FUNCTION (CF) OF AGGREGATED INTERFERENCE  $\Psi(\omega) = \mathbb{E}[e^{j\omega I}]$ .

where  $w \sim CN(0, \sigma_w^2/N)$  is the additive Gaussian noise with power  $\sigma_w^2/N$  after the array gain, and

$$\iota = \sum_{i=1}^{\infty} \frac{\beta_i}{(R_i^2 + h^2)^{\frac{b}{2}}} G(\phi_i, \theta_i) x_i. \quad (4)$$

is the aggregated interference originated from PPP distributed interfering UEs with density  $\lambda$ , all signals generated by all UEs are  $x_i \sim CN(0, 1)$ . We assume that the aggregate interference power  $I = |\iota|^2$  is typically  $\mathbb{E}[I] \gg \sigma_w^2/N$  as macro-cell network [15]. This assumption is relaxed in Sect. V, since in high frequencies, the noise is not negligible in small cells, specially in presence of blockage [36].

The outage analysis depends on the PDF of the aggregated interference (4) for PPP distribution of UEs having each polar coordinates  $(R_i, \theta_i)$ . The PDF of  $I$  without any array-gain for interference mitigation (here is a specific case with  $G^2(\phi_i, \theta_i) = 1$  for any  $i$ ) and  $h = 0$  has been extensively investigated in the literature (see e.g, [9], [37], [38]). The scope here is to evaluate the PDF of aggregated interference  $I$  for UcylA and  $h \geq 0$ . The  $N_c \times N_v$  UcylA is the most general case as UCA is when  $N_v = 1$  and the single antenna is when  $N_c = N_v = 1$ , as sketched in Table I, with the corresponding references or Sections for the analytic form of CF. Notice that the density  $\lambda$  refers to the number of *active* UEs per square meters coexisting on the same time-frequency and, depending on the specific radio resource allocation strategies, is likely to be meaningfully lower than effective crowd density [39].

The average probability of successful connection experienced by the UE of interest in  $(\phi_o, R_o)$  depends on a certain threshold  $T$ , on fading fluctuation  $|\beta_o|^2$ , and on the overall

interference  $I$ . The service probability from the distribution of  $I$

$$P_s(R_o|R_{max}) = F_I \left( \frac{|\beta_0|^2 G^2(\phi_0, \theta_0)}{T(R_o^2 + h^2)^b} \right), \quad (5)$$

where  $F_I(x) = \Pr(I < x)$  is the CDF. The service probability (5) is for the interference power  $I$  which accounts for the randomness of the position of the interferers according to the PPP model within a certain radius  $R_{max}$  and fading. The fluctuations of the interferers  $|\beta_i|$  is embodied in the CF derivations (Sect.III). The reference user in  $(R_o, \phi_o)$  is considered as deterministic for the computations of the (conditional) service probabilities, but whenever necessary for the unconditional probability, it can be assumed as PPP distributed as for the other interferers. Notice that the service probability  $P_s(R_o|R_{max})$  depends on the CDF of the aggregated interference  $I$  to be evaluated for the PPP distribution of active interferers, the array-type and its height  $h$ , as evaluated next section from CF analysis. For the unconditional service probability accounting for the fading of the user of interest, one should evaluate the expectation

$$\tilde{P}_s(R_o|R_{max}) = \mathbb{E}_{|\beta_0|^2} [P_s(R_o)]. \quad (6)$$

Differently from the interference analysis that aggregates multiple (and many) interfering contributions into the CF of  $I$ , (6) depends on the specific PDF of  $\beta_0$  thus making the service (or outage) analysis distribution-dependent for the UE of interest, see e.g [23], [40]. Therefore, the fast-fading contribution  $\beta_0$  is neutrally modelled here as  $\beta_0 = 1 \times e^{j\epsilon}$  with  $\epsilon \sim \mathcal{U}(0, 2\pi)$ , further derivations for arbitrary fading  $\beta_0$  are out of the scope here.

### III. CF OF THE AGGREGATED INTERFERENCE IN LOS

In this section, it is derived the CF of the aggregate interference in presence of LOS links first for the general case of  $N_c \times N_v$  UcyLA, then simplified for the UCA and single antenna. The focus of this paper is to infer the behaviour of the interference and coverage w.r.t. height and arrangements of the antenna array. The mmW channel modelling is first LOS-only, then is enriched with mixed LOS and NLOS links in Sect.V.

#### A. Uniform Cylindrical Arrays

$N_c \times N_v$  UcyLA is composed of  $N_v$  uniformly spaced rings consisting of  $N_c$  antennas each arranged in a cylinder shape (Fig. 1). The interference power  $I$  originated from a coverage radius  $R_{max} \rightarrow \infty$  represents the largest possible interference for a density  $\lambda$  and thus it is the upper bound of the interference  $I$  when  $R_{max} < \infty$ , the service probability (5) depends

on  $R_{max}$  and it is lower bounded:  $P_s(R_o|R_{max}) \geq P_s(R_o|R_{max} \rightarrow \infty)$ . The computation of the CF of the aggregate interference one should consider the entire gain pattern of the UcyLA (1, 2). Let  $R_{max} \rightarrow \infty$ , the aggregate interference power is

$$I = \sum_{i=1}^{\infty} \frac{|\beta_i|^2}{(R_i^2 + h^2)^b} \tilde{G}^2(R_i, \phi_i), \quad (7)$$

where the served UE is in  $(\theta_o, \phi_o) = (0, 0)$  for analytical notation convenience, and the beam-forming gains are reformulated in term of azimuth ( $\phi_i$ ) and elevation ( $\theta_i = \arctan(h/R_i)$ ) angles

$$\tilde{G}(R_i, \phi_i) = G_c^2(\phi_i) G_v^2(\arctan(h/R_i)) \quad (8)$$

The fluctuations' power  $|\beta_i|^2$  are independent of interfering users and identically distributed (iid). The randomly distributed interfering UEs in  $\phi_i \in [0, 2\pi)$  can be partitioned into a set of  $K$  disjoint angular sectors  $\Phi_1, \Phi_2, \dots$  such that  $\cup_k \Phi_k \equiv [0, 2\pi)$ , where  $K$  is large enough so that the array gain  $G_c(\Phi_k)$  in each sector can be considered as constant. The aggregate interference power (7) is

$$I = \sum_{k=1}^K \sum_{\phi_i \in \Phi_k} \frac{|\beta_i|^2}{(R_i^2 + h^2)^b} \tilde{G}^2(R_i, \phi_i) \simeq \sum_k I_k, \quad (9)$$

where

$$I_k = \sum_{i \in \Phi_k} \frac{|\beta_i|^2}{(R_i^2 + h^2)^b} \tilde{G}^2(R_i, \Phi_k). \quad (10)$$

The CF for the interference within the  $k$ th angular sector follows from Campbell's theorem as in [9]

$$\Psi_{I_k}(\omega) = \exp \left( -\frac{2\pi}{K} \lambda \int_0^{\infty} \left[ 1 - \Psi_{|\beta|^2} \left( \omega \frac{\tilde{G}^2(r, \bar{\phi}_k)}{(r^2 + h^2)^b} \right) \right] r dr \right), \quad (11)$$

where  $\Psi_{|\beta|^2}(\omega) = \mathbb{E}[e^{j\omega|\beta|^2}]$  is the CF of  $|\beta|^2$ . Defining  $\omega (r^2 + h^2)^{-b} = t$  and solving for  $t$  one gets (for  $\alpha = 1/b$ )

$$\Psi_{I_k}(\omega) = \exp \left( -\frac{\pi}{K} \lambda \alpha |\omega|^\alpha \int_0^{|\omega|/h^{2b}} \frac{1 - \mathbb{E}_{|\beta|^2}[e^{jt|\beta|^2 \tilde{G}^2(f(t), \Phi_k) \text{sign}(\omega)}]}{t^{\alpha+1}} dt \right). \quad (12)$$

where  $f(t) = (|\omega|^{1/b} t^{-1/b} - h^2)^{1/2}$  follows from the conversion from variable  $r$  to  $t$ . Since the array gain is a function of  $t$ , this expression can only be solved numerically. One way to make the CF tractable is by uniformly dividing the elevation angle  $\theta_v \in (0, \pi/2]$  into  $M$  angular sectors of  $\Delta_v = \pi/2M$  width, each sector is centered in  $\tilde{\theta}_m = \frac{\pi}{2} \left( \frac{2(M-m)+1}{2M} \right)$ , and the width  $\Delta_v$  is small enough to let the array gain in every angular sector (2) be constant  $G_v^2(\tilde{\theta}_m)$ . The array gain is constant on every annulus (ring) shaped areas with unequal widths (non-uniform rings division for uniform elevations  $\tilde{\theta}_m$ ). These rings are centered in the radial



distance of the intersection of the  $m$ th bisector  $\tilde{\rho}_m = h/\tan(\theta_m - \frac{\pi}{4M})$ , so that the array gain in  $k$ th wedge and  $m$ th ring is  $\tilde{G}^2(\tilde{\rho}_m, \Phi_k)$ . Within the  $k$ th wedge and  $m$ th ring the array gain is constant and the interference originated  $I_{k,m}$  has the CF

$$\Psi_{I_{k,m}}(\omega) = \exp\left(-\frac{\pi}{K}\alpha\lambda|\omega|^\alpha \int_{\tau_{m+1}}^{\tau_m} \left[\frac{1 - \mathbb{E}_{|\beta|^2}[e^{jt|\beta|^2\tilde{G}^2(\tilde{\rho}_m, \Phi_k)\text{sign}(\omega)}]}{t^{\alpha+1}}\right] dt\right), \quad (13)$$

where  $\tau_m = |\omega|/(h^2 + \rho_m^2)^b$ . The CF of the aggregate interference statistically independent on all  $K$  wedges and  $M$  rings is  $\Psi_I(\omega) = \prod_{m=0}^{M-1} \prod_{k=0}^{K-1} \Psi_{I_{k,m}}(\omega)$  and it can be shown to reduce to <sup>1</sup>

$$\Psi_I(\omega) = \exp(-\lambda 2\pi R_{max}^2) \exp\left(-\frac{\pi\lambda}{C_\alpha} |\omega|^\alpha (1 - j\text{sign}(\omega) \tan \frac{\pi\alpha}{2}) P_G(\omega)\right) \quad (14)$$

with  $C_\alpha^{-1} = \Gamma(1 - \alpha) \cos(\pi\alpha/2)$  and

$$P_G(\omega) = \frac{\bar{\beta}^{2\alpha}}{K} \sum_{k=0}^{K-1} \sum_{m=0}^{M-1} \tilde{G}^{2\alpha}(\tilde{\rho}_m, \Phi_k) [P(-\alpha, -j|\omega|\xi(\tilde{\rho}_m, \Phi_k)) - P(-\alpha, -j|\omega|\xi(\tilde{\rho}_{m+1}, \Phi_k))]. \quad (15)$$

We used a compact notation for different moments of fading  $\bar{\beta}^c = \mathbb{E}[|\beta|^c]$ , and  $P(x, z) = \int_0^z t^{x-1} e^{-t} dt / \Gamma(x)$  in (15) is the normalized incomplete Gamma function ratio and

$$\xi(r, \phi) = \frac{\tilde{G}^2(r, \phi) \bar{\beta}^2}{(h^2 + r^2)^b}. \quad (16)$$

The relationship (15) for  $M \rightarrow \infty$  and  $R_i \leq R_{max} < \infty$  it reduces, after some calculus, into

$$P_G(\omega) = \frac{2b}{(-j\omega)^\alpha \Gamma(-\alpha)} \int_0^{R_{max}} \left( \int_0^{2\pi} e^{j|\omega|\xi(r, \phi)} \frac{d\phi}{2\pi} \right) r dr. \quad (17)$$

This relation (17) completes the CF of aggregated interference (14). The PDF and the CDF of the interference  $I$  is obtained by numeric inversion. For  $h \rightarrow 0$  the UcyLA degenerates into UCA on the ground, and the distribution of  $I$  is alpha-stable for  $R_{max} \rightarrow \infty$  (Sect.III-B). As seen, the general amplitude fluctuations  $\beta_i$  of the interferers is embodied in the derivation of the CF (whose values depend on the specific fading model chosen), however, for the numerical calculations throughout the paper, the fading power  $\bar{\beta}^2$  is neglected because it is averaged out in the SG over the summation of the interference for all UEs (the fading power for the user of interest  $|\beta_0|^2$  does not average out).

*Remark 1:* Although the CF of aggregated interference (14) for UcyLA depends on (17), its numerical computation has some trade-offs. The granularity of numerical integration basically depends on the main beamwidth: the azimuth  $K = N_c$  is a safe choice with good accuracy,

<sup>1</sup>The solution of the integral  $\int_0^{|\omega|/h^{2b}} \left[ \frac{1 - e^{j\mu t}}{t^{\alpha+1}} \right] dt = \lim_{\epsilon \rightarrow 0} (-j\mu)^\alpha \Gamma(-\alpha, -j\mu t) - \frac{1}{\alpha t^\alpha} \Big|_{t=\epsilon}^{t=|\omega|/h^{2b}}$ , for any constant and real  $\mu$ , and  $0 < \alpha < 1$ .

while for the elevation angle  $M = N_v/2$  to  $M = N_v/4$  is acceptable ( $M = N_v/2$  is a safe choice for large  $\lambda$  say  $\lambda > 0.1$ ). Thus, the complexity decrease w.r.t. massive integration, and in fact, this method would be a good way of decreasing the computation complexity. Alternatively, whenever one uses the beam gain approximation models like the flat-top model [24], the summation reduces straightforwardly to two terms, and it would be quite fast in terms of computations for network analyses.

*Remark 2:* The array gain (2) of vertical ULA is critical for the analytical tractability of the CF derivation, and the use of  $N_v > 1$  could be questionable for height too small. The array gain (2) holds true when the array aperture is compact compared to array height  $h$  to have a plane wave-front. In practice, for mmW communications at a frequency around (or larger) 30GHz the wavelength is approx (or smaller than ) 1cm, and for  $N_v = 10$  antennas, the array aperture for half-wavelength antennas' spacing is 5cm (or less). In the scenario in Fig. 1 the height should be above the people heights and for  $h > 2m$  the approximation that array aperture is compact ( $2m \gg 5cm$ ) holds true.

### B. Specific Cases

**UCA:** UCA is a special case of UcyLA for  $N_v = 1$  (i.e.,  $G_v(\theta) = 1$ ). The statistical distribution of aggregated interference  $I$  for UCA can be adapted by considering  $R_{max} \rightarrow \infty$ , although it can be extended to  $R_{max} < \infty$ . In UCA there is no radial mitigation of the interference, but it is only along the azimuth. After simplifying the relation (14) and resolving the singularity (Appendix A), it yields to:

$$\Psi_I(\omega) = \exp\left(-\frac{\pi\lambda}{C_\alpha} |\omega|^\alpha \left(1 - j\text{sign}(\omega) \tan \frac{\pi\alpha}{2}\right) P_{G_c(\omega)} + \pi\lambda h^2\right), \quad (18)$$

where

$$P_{G_c(\omega)} = \frac{\bar{\beta}^{2\alpha}}{K} \sum_{k=1}^K G_c^{2\alpha}(\Phi_k) P\left(-\alpha, -j|\omega| \frac{G_c^2(\Phi_k) \bar{\beta}^2}{h^{2b}}\right) \quad (19)$$

The limit for  $K \rightarrow \infty$  angular sectors is

$$P_{G_c(\omega)} = \frac{\bar{\beta}^{2\alpha}}{2\pi} \int_0^{2\pi} G_c^{2\alpha}(\phi) P\left(-\alpha, -j|\omega| \frac{G_c^2(\phi) \bar{\beta}^2}{h^{2b}}\right) d\phi \quad (20)$$

and this term has to be evaluated numerically.

Considering as special case  $h \rightarrow 0$ , it is  $P_{G_c} \rightarrow 1$ , so the frequency dependence of  $P_{G_c}$  vanishes, and the aggregated interference in the  $k$ th angular sector is skewed alpha-stable<sup>1</sup>:

$$G_c^2(\Phi_k) \sum_{i \in \Phi_k} \frac{|\beta_i|^2}{R_i^{2b}} \sim \mathcal{S} \left( \alpha = \frac{1}{b}, \gamma_k \right), \quad (21)$$

where  $\gamma_k = \frac{\Delta\phi_k}{2} \lambda G_c^{2\alpha}(\Phi_k) \frac{\bar{\beta}^{2\alpha}}{C_\alpha}$  and  $C_\alpha^{-1} = \Gamma(1 - \alpha) \cos(\pi\alpha/2)$ . The overall interference reduces to the sum of skewed stable random terms (straightforwardly from [41, eq.(1.8)])

$$I = \sum_k I_k \sim \mathcal{S} \left( \alpha = \frac{1}{b}, \gamma_c \right) \quad (22)$$

where the total dispersion for UCA becomes

$$\gamma_c = \pi \lambda \frac{\bar{\beta}^{2\alpha}}{C_\alpha} \cdot \frac{\int_0^{2\pi} G_c^{2\alpha}(\phi) d\phi}{2\pi}, \quad (23)$$

assuming sectors  $\Delta\phi_k \rightarrow 0$ . Therefore, the aggregated interference for UCA and  $h = 0$  is skewed alpha-stable. However, increasing the height  $h$ , the distribution deviates from alpha-stable as detailed later. Comparing this result with [9] one notices an additional term that depends on the UCA array gain  $G_c^2(\phi)$  that mitigates the mean level of interference in skewed stable distribution. As before, the fading powers of the interferers is embodied in the derivations, but they will average out in summation of the interference power over all of the UEs (the fading amplitude of each signal from each UE depends on the chosen fading model), while the fading power from the user of interest remains effective in the calculation of the service probability.

**Point antenna:** a single point antenna can be considered as a special case of a UCA, where  $N_c = 1$  that leads to an isotropic gain. Placing the antenna at height  $h > 0$  the CF of the aggregated interference power can be achieved by simplifying (18) as

$$\Psi_I(\omega) = \exp \left( -\frac{\pi\lambda}{C_\alpha} |\omega|^\alpha \bar{\beta}^{2\alpha} P(-\alpha, -j|\omega| \frac{\bar{\beta}^2}{h^{2b}}) (1 - j \text{sign}(\omega) \tan \frac{\pi\alpha}{2}) + \pi\lambda h^2 \right). \quad (24)$$

This CF generalizes the CF for  $h = 0$  in [9] and both trivially coincides for  $h \rightarrow 0$ . The term of  $P(-\alpha, -j|\omega| \frac{\bar{\beta}^2}{h^{2b}})$ , depending on  $\omega$ , will increase from initial value of  $P(-\alpha, -j|\omega| \frac{\bar{\beta}^2}{h^{2b}}) = 1$  at  $h = 0$ .

<sup>1</sup> $\mathcal{S}(\alpha, \gamma)$  denotes the skewed stable distribution with characteristic exponent  $\alpha \in (0, 2]$ , unitary skewness, and scale parameter (or dispersion)  $\gamma \geq 0$  with a characteristic function

$$\mathbb{E}[e^{j\omega x}] = \begin{cases} \exp[-\gamma|\omega|^\alpha (1 - j \text{sign}(\omega) \tan \frac{\pi\alpha}{2})] & \alpha \neq 1 \\ \exp[-\gamma|\omega|^\alpha (1 + j \frac{2}{\pi} \text{sign}(\omega) \ln |\omega|)] & \alpha = 1 \end{cases}$$

### C. Analysis of AP height

To gain an insight regarding the effect of the height of the antenna, it is useful to evaluate the mean aggregated interference that, for simplicity, is for UCA. The mean  $\mathbb{E}[I]$  follows from the CF properties:

$$\mathbb{E}[I] = \frac{\pi\lambda\alpha^2}{(\alpha-1)} h^{2(1-b)} \bar{\beta}^2 \bar{G}_c^2. \quad (25)$$

where  $\bar{G}_c^2 = \frac{1}{2\pi} \int_0^{2\pi} G_c^2(\phi) d\phi$  is mean power gain. The aggregated interference power decreases as the height of the antenna increases, and increases with density  $\lambda$ . As an illustrative example Fig.2 shows the received signal power and the aggregated interference power case for the transmit power of all the UEs equal 0 dBm, and the normalized array gain for the user of interest located at distance  $R_0$  is maximum (i.e.  $G_c(\phi_0) = 1$ ). The received useful signal power  $P_{rx}$  by a single UE is:

$$P_{rx} = \frac{|\beta_0|^2}{(R_0^2 + h^2)^b}, \quad (26)$$

where the amplitude  $\beta_0$  considers the path-loss at distance 1m:  $\beta_0 = 4\pi F_c/c$  for  $c = 10^8 m/s$  and  $F_c$  is the carrier frequency (here  $F_c = 28$  GHz). The mean interference power follows (25). It can be observed that for large thresholds  $[T]_{dB} = \{4, 5\}$  the average interference power is larger than the signal power and the system is in outage for every AP height. For smaller thresholds, the AP serves the target UE for a range of AP heights. For example at  $[T]_{dB} = 0$ , the serving range of AP height is approximately  $1m < h < 33m$ . At around  $h = 1m$ , the difference of target UE signal power and mean aggregated interference is zero. For AP height range  $1m < h < 9m$ , this difference increases, and for AP height range of  $9m \leq h < 33m$  the difference decreases, while for  $33m < h$  the user is in outage.

### D. Numerical validation on aggregated interference

The CF derived for each of the arrays is validated here by numerically computing the PDF and CDF from inverse Fourier methods tailored for statistical distributions to be accurate on the tails of the distributions [42], [43]. The service probability (5) is the comparison metric adopted here for the validation of the CFs in the previous sections, by considering a LOS system with  $|\beta_0|^2 = 1$  and threshold  $T = 1$  (or 0dB). The transmitting interferers are numerically generated as random PPP with a maximum radius  $R_{\max}^{(\text{num})}$  specified below for every Monte-Carlo iteration and are affected by the array gain  $G(\phi, \theta) = G_c(\phi)G_v(\theta)$  (see (1) and (2)) keeping fixed the radial position  $R_0$  for the UE of interest as aggregated interference is isotropic vs. azimuth.

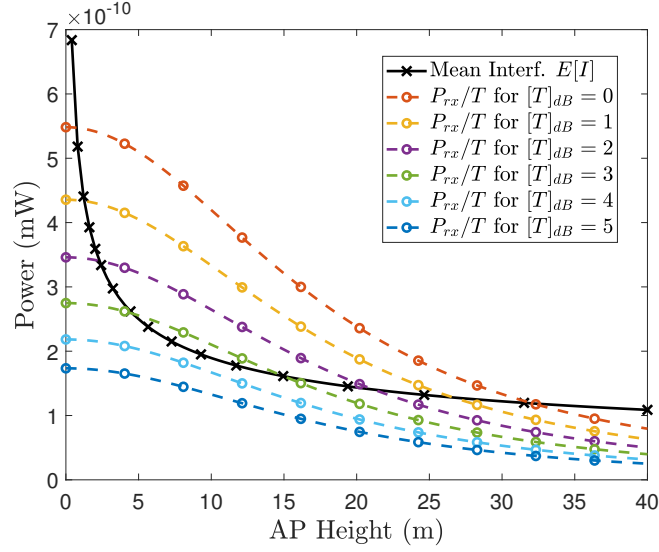


Figure 2. Received Power and mean aggregated Interference power vs. AP height  $h$ , for a target UE located at  $R_0 = 20\text{m}$  equipped with a uniform circular array (UCA) with  $N_c = 128$  that has average power gain  $\bar{G}_c^2 = 0.012$ . Parameters: SINR threshold  $[T]_{dB} = \{0, 1, 2, 3, 4, 5\}$ , interferers' density  $\lambda = 5 \times 10^{-3} \text{ m}^{-2}$ , path-loss exponent  $2b = 2.4$ , central frequency  $F_c = 28 \text{ GHz}$ , and transmit power  $P_{tx} = 0\text{dBm}$ .

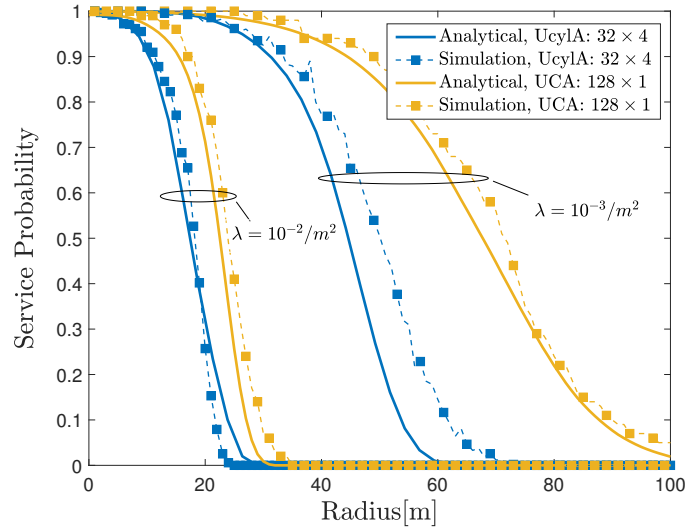


Figure 3. Service probability vs. radius  $R_o$  for varying  $\lambda = \{10^{-3}, 10^{-2}\} \text{ m}^{-2}$  where the access point (AP) employs a UCA with  $N_c = 128$  or a UcyIA with  $N_c \times N_v = 32 \times 4$ . Parameters:  $R_{\max}^{(\text{num})} = 200 \text{ m}$ ,  $[T]_{dB} = 0$ ,  $|\beta_0|^2 = 1$ ,  $2b = 2.6$ ,  $h = 10 \text{ m}$ .

Fig. 3 demonstrates the comparative analysis of UcyIA and UCA showing the  $P_s(R_o)$  vs. radius  $R_o$  using  $\Psi_I(\omega)$  for UcyIA in (14) and for UCA in (18) where the total number of antennas is preserved in all cases ( $N_c \times N_v = 128$ ) and the signal-to-noise-and-interference (SINR) threshold  $[T]_{dB} = 0$ . In case of UCA, the analytical curves are a lower bound of

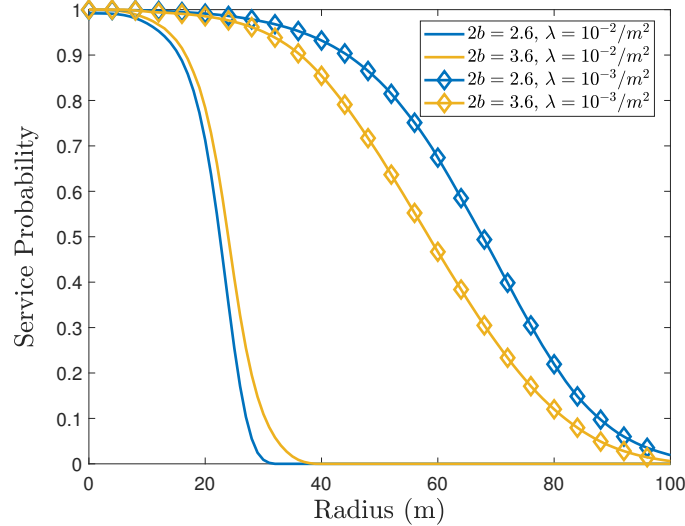


Figure 4. Service probability vs. radius  $R_o$  for varying  $\lambda = \{10^{-2}, 10^{-3}\} m^{-2}$  where the AP employs a UCA with  $N_c = 128$ . Parameters:  $R_{\max}^{(\text{num})} = 200 m$ ,  $[T]_{dB} = 0$ ,  $|\beta_0|^2 = 1$ ,  $2b = 2.6$  and  $2b = 3.6$ ,  $h = 10 m$ .

$P_s(R_o)$  when compared to the numerical simulation with  $R_{\max}^{(\text{num})} \ll R_{\max}$ . Simulations can show that for UCA, increasing  $R_{\max}^{(\text{num})} > 200 m$  (not shown here), the numerical  $P_s(R_o)$  attains the analytic ones. Service probability  $P_s(R_o)$  decreases for increasing served UE position  $R_o$  as interference from  $\lambda$ -density interferers dominate. For smaller density (here  $\lambda = 10^{-3} m^{-2}$ ) the service probability  $P_s(R_o) > 0.5$  up to 70 m For UCA and around 50m for UcyLA. It can be noticed that in the given scenario with given parameters, the UCA seems to surpass the UcyLA from service probability point of view.

Increasing the path-loss exponent ( $2b = 3.6$  in Fig. 4) affects the service probability as aggregated interference is more attenuated for far away interferers, and it is more effective for denser users (i.e., for larger  $\lambda$  the increase of the path-loss is more beneficial for  $P_s(R_o)$ , while detrimental for small  $\lambda$ ).

Once validated the analytical model, one might investigate the  $N_c$  vs.  $N_v$  arrangement of UcyLA for a given total number of antennas  $N_c N_v$  (e.g., for the same complexity of the radio frequency circuitry). The cylinder arrangement of the UcyLA can be tall ( $N_c < N_v$ ), fat ( $N_c > N_v > 1$ ) or just a ring ( $N_v = 1$ ) and the optimum array geometry for service probability depends on different parameters like the SIR threshold ( $T$ ), path-loss exponent ( $b$ ), the antenna (or users) height  $h$ , and the directivity of every antenna element (not considered here). The metric used herein is the ratio of the served users in a certain area ( $2\pi\lambda \int_0^{\bar{R}} P_s(r)rdr$ ) to the total average users ( $\pi\bar{R}^2\lambda$ ) here assumed PPP distributed, it is also referred as average

service probability

$$\bar{P}_s = \frac{2 \int_0^{\bar{R}} P_s(r) r dr}{\bar{R}^2}. \quad (27)$$

In the following examples, we maintaining the total number of antennas  $N_c \times N_v = 256$ , changing the ratio of UCA and vertical antennas.

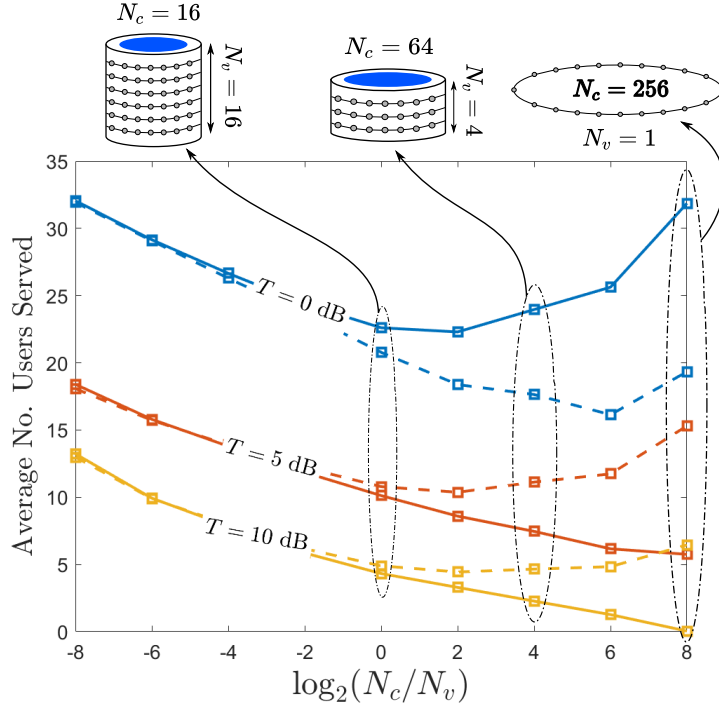


Figure 5. Average service probability  $\bar{P}_s$  vs antennas ratio  $\log_2(N_c/N_v)$ , within  $\bar{R} = 50$  m while keeping constant the total number of antennas ( $N_c N_v = 256$ ) for different thresholds  $[T]_{dB} = \{0, 5, 10\}$ , AP height  $h = 5$  m,  $|\beta_0|^2 = 1$ ,  $\lambda = 5 \times 10^{-2} m^{-2}$ : Solid lines correspond to  $2b = 2$  and dashed lines corresponding to  $2b = 3.6$ .

Figure 5 illustrates  $\bar{P}_s$  vs. the antennas ratio  $\log_2(N_c/N_v)$ , varying the SINR threshold  $[T]_{dB} = \{0, 5, 10\}$  for small and large path-loss exponents  $2b = \{2, 3.6\}$ . It can be seen that in the given scenario, by increasing the threshold  $T$ , UCA performs worse. Note that in this setup, the UEs are very dense ( $\lambda = 5 \times 10^{-2} m^{-2}$ ). It can be shown that for smaller UE densities, UCA outperforms the UcyLA. Fig. 6 shows a similar example of  $\bar{P}_s$  vs. the antennas ratio  $\log_2(N_c/N_v)$ , fixing the threshold  $[T]_{dB} = 5$  and varying the AP height  $h = \{5, 10, 15, 20\}$  m. Clearly by increasing the AP height, the usage of UcyLA becomes more advantageous in terms of  $\bar{P}_s$  and it is more meaningful to use vertical beamforming, while for smaller heights it is preferable to use a larger circular array. However, it can be observed that in this scenario where UEs are dense, the service probability in general decreases by increasing the height. Thus, it is preferable to use an AP with smaller height.

Fig. 7 shows the effect of UEs density  $\lambda$ . It is seen that for areas that are not so dense, a

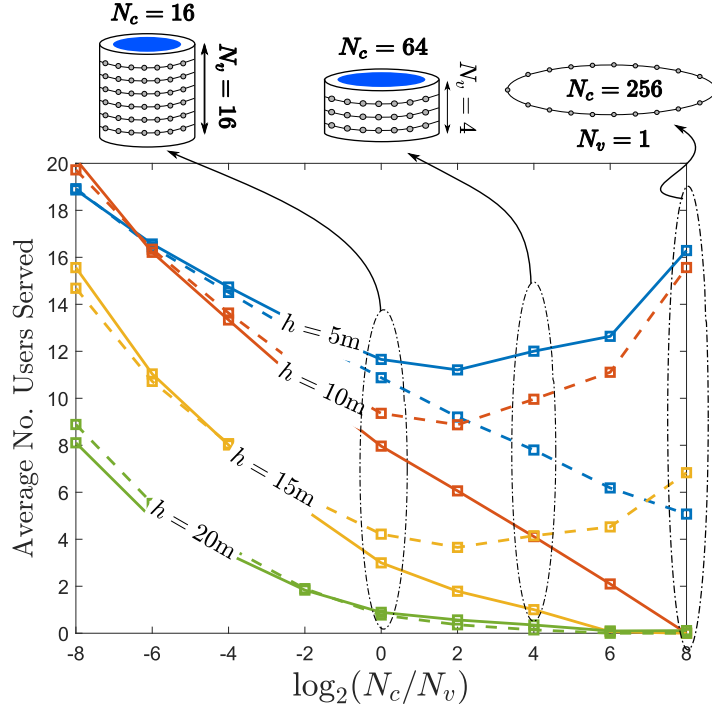


Figure 6. Average service probability  $\bar{P}_s$  vs antennas ratio  $\log_2(N_c/N_v)$ , within  $\bar{R} = 100$  m while keeping constant the total number of antennas ( $N_c N_v = 256$ ) for different array height  $h = \{5, 10, 15, 20\}$  m, threshold  $[T]_{dB} = 5$ ,  $|\beta_0|^2 = 1$ ,  $\lambda = 5 \times 10^{-2} \text{ m}^{-2}$ : Solid lines correspond to  $2b = 2$  and dashed lines corresponding to  $2b = 3.6$ .

UCA is mildly preferable. However for more dense areas, a UcyLA would be more preferable depending on different parameters. It can be shown that changing every one of the above-mentioned parameters affects the shape of the  $\bar{P}_s$  curves. Furthermore, the constraint of ground UEs is also responsible for results. UcyLAs are favored in case UEs have arbitrary heights (usually indoor UEs are at arbitrary heights, while in high frequencies we target, penetration loss is too high).

A pragmatic conclusion from these evaluations is that for most real-life scenarios where UEs densities are not too high, it is beneficial to invest in UCA arrangement rather than UcyLA. There are two reasons supporting this result: i) the most powerful interferers are in the vicinity of the AP, while the minimum separable angle by the ULA is  $\Delta\theta_{min} \approx \frac{\lambda}{N_v d_v \cos(\theta_0)}$ , where  $d_v$  is the vertical inter-element spacing, and  $\theta_0$  is the target elevation; ii) even if the resolution was not angle dependent, dividing the whole elevation plane into small portions of same width is emphasizing the same way to near and to far UEs, while the most powerful UEs are closer ones. In the rest of the numerical examples in the paper, we focus on the usage of UCA, since the target threshold used is set to  $[T]_{dB} = 0$  and the interferers' density used are not extremely high, that justifies the usage of a UCA over UcyLA.



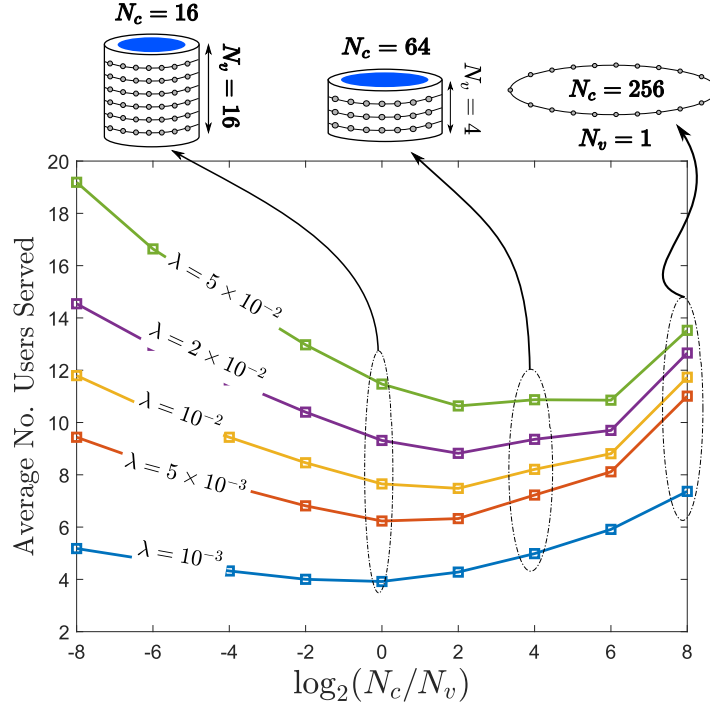


Figure 7. Average service probability  $\bar{P}_s$  vs antennas ratio  $\log_2(N_c/N_v)$ , within  $\bar{R} = 100$  m while keeping constant the total number of antennas ( $N_c N_v = 256$ ) for different interferers' density  $\lambda = \{1, 5, 10, 20, 50\} \times 10^{-3} \text{ m}^{-2}$ , threshold  $[T]_{dB} = 5$ ,  $|\beta_0|^2 = 1$  and  $2b = 2$

*Remark 3:* Note that although the left most parts of the curves (i.e. corresponding to a ULA or a very tall UcyLA) are shown in the figures, in practice they are not feasible to deploy. Therefore, one might consider the range  $N_c > N_v/8$  as practical solution.

#### IV. STATISTICAL CHARACTERIZATION OF THE AGGREGATED INTERFERENCE POWER

The aggregate interference  $I$  in Sect.III-A for UcyLA and arbitrary height  $h > 0$  is complex to be computed or analytically in a closed-form; herein we propose a methods for statistical approximation of the aggregate interference CF. We show that the aggregated interference power for an array of antenna located at arbitrary height, can be approximated by a weighted mixture of two stable distributions and we detail herein the equivalent CF.

In order to get a deeper insight into the distribution in an arbitrary height, one can start from the Taylor series of the argument of the CF ( $\Psi_I(\omega)$ ). For example, the series for a UCA with arbitrary height and  $|\beta_i| = 1$ , follows from the CF (18) that, with some simplifications, yields:

$$\Psi_I(\omega) = \exp(\pi\alpha\lambda\Xi(\alpha, \omega)), \quad (28)$$

where the Taylor series is

$$\Xi(\alpha, \omega) = \frac{1}{K} \sum_{k=1}^K \sum_{i=1}^{\infty} \frac{\left(\frac{1}{h^{2b}}\right)^{i-\alpha}}{(i-\alpha)!} (j\omega\bar{\beta}^2 G_c^2(\Phi_k))^i. \quad (29)$$

Let's define  $G_{avg}^{(z)} = \frac{1}{K} \sum_{k=1}^K G_c^{2z}(\Phi_k)$ , for  $h = 0$  relation (29) simplifies to

$$\Xi(\alpha, \omega) = (-j\omega)^\alpha \Gamma(-\alpha) \bar{\beta}^{2\alpha} G_{avg}^{(\alpha)}. \quad (30)$$

For very large heights  $h \gg 0$  in (28), the terms with higher index  $i$  get negligible, and it can be approximated with only the first two terms, which would make the CF ( $\Psi_I(\omega)$ ) be a Gaussian distribution<sup>3</sup>. In order to evaluate the appropriate CF for any  $h > 0$  one isolates the behaviour vs.  $j\omega$  from  $\Xi(\alpha, \omega)$  as:

$$\Xi(\alpha, \omega) = \Xi'(\alpha, \omega) + \frac{\left(\frac{1}{h^{2b}}\right)^{1-\alpha}}{1-\alpha} j\omega\bar{\beta}^2 G_{avg}^{(1)}, \quad (31)$$

where the second term (corresponding to  $i = 1$  in (28)) is a shift or location parameter. The behavior of the real part of  $\Xi(\alpha, \omega)'$  reveals the corresponding exponent of  $\omega$ , for every defined  $\omega$ . The reason to separate  $\Xi(\alpha, \omega)$  in two parts is that we need to omit the shift, to be able to visualise the exponent of the  $\omega$  within the distribution. For large  $h$ ,  $\Xi'(\alpha, \omega)$  vs  $\omega$  behaves as  $\omega^2$ , for very small  $h$  behaves as  $\omega^\alpha$ , while for medium heights it has two different slopes based on  $\omega$ . The transition  $\omega$  where the behaviour changes is  $\bar{\omega}$ , that depends on the height, the path-loss exponent, UEs density and array gain. Having gained insight regarding the behavior vs  $\omega$  and  $\bar{\omega}$  which is explained in further text,  $\Xi(\alpha, \omega)$  can be approximated as:

$$\Xi(\alpha, \omega) = W_1(\omega) \times a(\omega) + W_2(\omega) \times (1 - a(\omega)), \quad (32)$$

where  $a(\omega)$  is a Heaviside step function, i.e.,  $a(\omega) = 1$  for  $\omega < \bar{\omega}$  and 0 otherwise (or some function with smoother transition), that acts as a switch between two cases with different behaviour:

$$W_1(\omega) \approx \frac{\left(\frac{1}{h^{2b}}\right)^{1-\alpha}}{1-\alpha} j\omega\bar{\beta}^2 G_{avg}^{(1)} - \frac{\left(\frac{1}{h^{2b}}\right)^{2-\alpha}}{2(2-\alpha)} \omega^2 \bar{\beta}^4 G_{avg}^{(2)} \quad (33)$$

$$W_2(\omega) = (-j\omega)^\alpha \Gamma(-\alpha) \bar{\beta}^{2\alpha} G_{avg}^{(\alpha)}, \quad (34)$$

where  $W_2$  coincides with the skewed-stable distribution (22). Relation (32) means that the CF is decomposable as

$$\Psi_I(\omega) = \exp(\pi\alpha\lambda W_1(\omega) a(\omega)) \cdot \exp(\pi\alpha\lambda W_2(\omega) (1 - a(\omega))). \quad (35)$$

<sup>3</sup>The CF of a Gaussian distribution  $\exp\left(j\mu\omega - \frac{\sigma^2}{2}\omega^2\right)$  with shift  $\mu$ .

Fig. 8 demonstrates the behavior of the real part of  $\Xi(\alpha, \omega)$  vs  $\omega$  for a single isotropic antenna and set of AP heights  $h = \{0, 2, 5, 20, 100\}m$ . It can be seen that by increasing the AP height, the breaking frequency  $\bar{\omega}$  increases, while for extremely large AP heights, it tends to infinite that is Gaussian distribution behavior. Fig. 9 is the same analysis, comparing a isotropic antenna with a UCA consisting of  $N_c = 16$  isotropic antennas for the set of AP heights  $h = \{0, 5\}m$ . It is observed that the slopes of the curves are maintained, while the breaking frequency is increased when using a UCA.

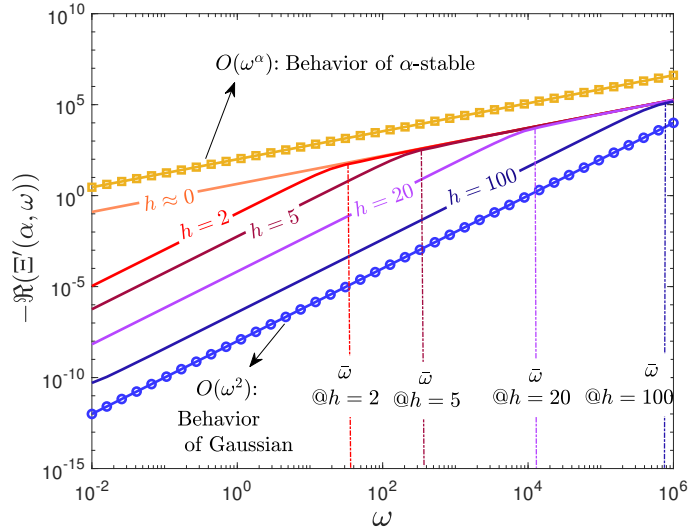


Figure 8. Real part of the  $\Xi(\alpha, \omega)'$  vs.  $\omega$  for  $2b = 2.6$  and  $\lambda = m^{-2}$ , with a single isotropic antenna for different heights of the array. The two guidelines are parallel with  $\omega^\alpha$  and  $\omega^2$ . For large heights,  $\Xi'(\alpha, \omega)$  vs  $\omega$  behaves as  $\omega^2$ , for very small heights it behaves as  $\omega^\alpha$ , while for medium heights it has two different slopes based on  $\omega$ .

One can approximate the CF for a UCA in every arbitrary height, given the knowledge about the transition frequency  $\bar{\omega}$ . Knowing the transition point  $\bar{\omega}$ , based on height  $h$  one may characterize with different statistical distributions for different  $\omega$ . Numerical formulation of  $\bar{\omega}$  vs. antenna height and other parameters can be investigated further. A rule of thumb for  $\bar{\omega}$  can be achieved as follows. Let  $S_i(\omega)$  denote the  $i$ -th term of the series (29) as:

$$S_i(\omega) = \frac{\left(\frac{1}{h^{2b}}\right)^{i-\alpha}}{(i-\alpha)!} \left(j\omega\bar{\beta}^2 G_{avg}^{(i)}\right)^i. \quad (36)$$

It is empirically observed that  $\bar{\omega}$  can be approximately achieved by imposing the condition  $S_2(\omega) = S_3(\omega)/\bar{\beta}^2$  and by solving for  $\omega$  and the  $\bar{\omega}$  can be achieved. Please note that this formula holds for normalized array gain. The rationale behind these conditions lies in the fact that for an  $\alpha$ -stable distribution and for height  $h = 0$  all the terms for  $i > 1$  tend to infinite, while for Gaussian distribution only the first three terms exist. In the mixture case,

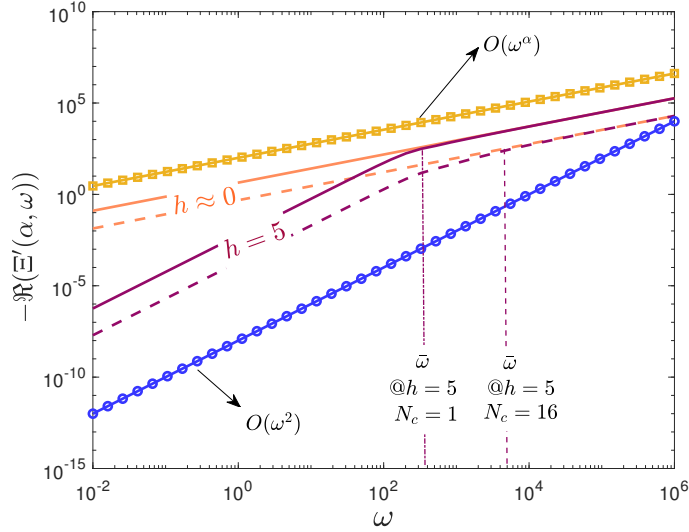


Figure 9. Real part of the  $\Xi(\alpha, \omega)'$  vs.  $\omega$  for  $2b = 2.6$  and  $\lambda = 1 \text{ m}^{-2}$ , comparing the UCA with single antenna. The two guidelines are parallel with  $\omega^\alpha$  and  $\omega^2$ : Solid lines correspond to a point antenna while dashed lines correspond to a UCA with  $N_c = 16$  isotropic antennas on a ring.

for  $\bar{\omega} < \omega$  behaviour resembles  $\alpha$ -stable. In the case of Fig. 8 the calculated  $\bar{\omega}$  for the AP heights of  $h = \{2, 5, 10, 100\} \text{ m}$  are respectively  $\bar{\omega} = \{32, 355, 13070, 858160\}$ , and in Fig. 9, the  $\bar{\omega}$  for AP height  $h = 5 \text{ m}$  for two cases of  $N_c = \{1, 16\}$  are respectively  $\bar{\omega} = \{355, 5688\}$ . Based on the figures, it can be noticed that these approximation are close to the real breaking points of the curves.

In practical systems, the height is known but other parameters such as the density of active users  $\lambda$  is not known, and some inaccuracies w.r.t. the ideal model might occur. We believe that the knowledge of a reasonable approximation of the distribution of the aggregated interference enables the possibility to measure the approximating alpha-stable distribution during multiple idle times of the communication intervals by any unsupervised learning method [44] being a practical on-the-fly method.

## V. OUTAGE ANALYSIS IN PRESENCE OF NLOS, NOISE AND BLOCKAGE

In the previous sections, we derived the CF of the aggregated interference power with different antenna array configurations, and characterized the distribution of the aggregated interference power. Moving toward the modelling of practical mmW and sub-THz systems, in this section, it is shown how the NLOS propagation, noise power and blockage can be integrated into the model.

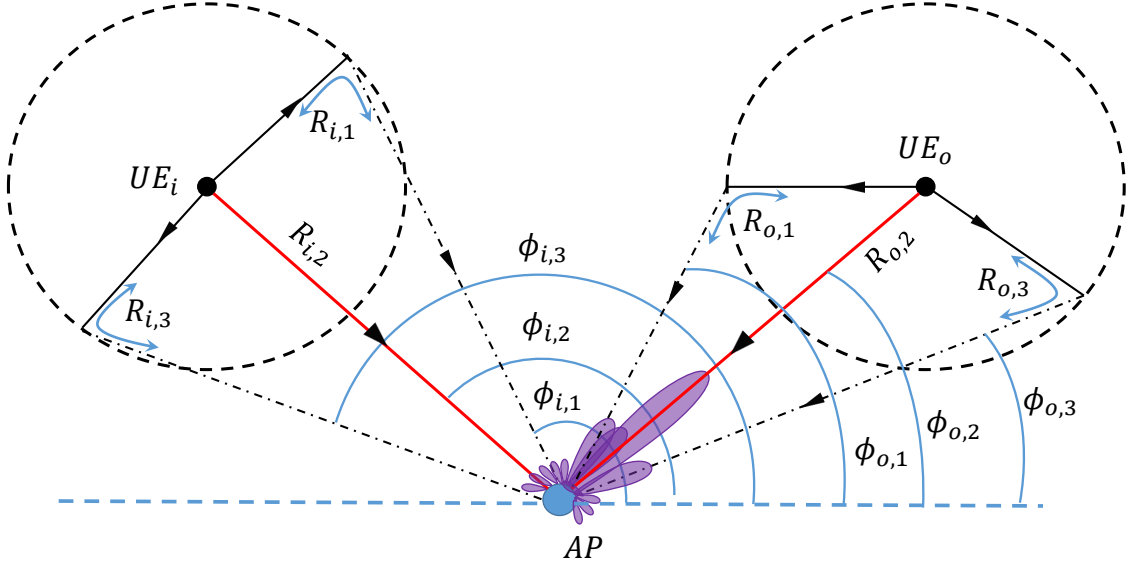


Figure 10. NLOS model: every user has few NLOS links in addition to a LOS link. LOS links are shown with thick red lines, and NLOS links are shown with dashed lines reflected back from the perimeter of a circle around the UE. Here the  $UE_o$  is the user of interest and  $UE_i$  is an interferer.

#### A. NLOS paths

Previous studies and measurement campaigns [45], have shown that the NLOS clusters of rays are present in mmW communications where they form sparse multipath faded channels. These paths can increase the amount of interference, but at the same time would lead to more useful signal received in the case of coherent reception of signal. On the other hand, diversity is an efficient way to compensate the blockage and to increase the reliability of communication systems.

#### B. NLOS paths

Let  $L$  be the total number of paths that the signal arrives from the user of interest to the same AP, the  $L \times 1$  set of signals  $\mathbf{y} = [y_1, y_2, \dots, y_L]^T$  after the multi-beam beamforming to each of the paths from the user of interest transmitting  $x$  is

$$\mathbf{y} = \mathbf{h}x + \boldsymbol{\nu} + \mathbf{w} \quad (37)$$

where  $[\mathbf{h}]_\ell = h_\ell = \beta_{o,\ell}/D_\ell^b$  for distance  $D_\ell = (R_{o,\ell}^2 + h^2)^{1/2}$  corresponding to the  $\ell$ th paths of arrival (in case  $\ell = 1$  it is the direct LOS link and  $R_{o,1} = R_o$  is the geometric distance between

the user of interest, while the distances for NLOS links are modelled later but  $R_{o,\ell} \geq R_o$ . The ensemble of the aggregated interference amplitudes from the PPP distributed interferers is  $\boldsymbol{\iota} = [\iota_1, \iota_2, \dots, \iota_L]^T$  that are independent and identically distributed (iid) random variables are obtained from a set of  $L$  beamforming toward the distinct angles  $\phi_{o,1}, \phi_{o,2}, \dots, \phi_{o,L}$  for LOS ( $\phi_{o,1}$ ) and NLOS ( $\phi_{o,2}, \dots, \phi_{o,L}$ ) of the user of interest, so that adapting 4 to this case with multipath for interference is:

$$\boldsymbol{\iota} = \sum_{i=1}^{\infty} \sum_{\ell=1}^L \frac{\beta_{i,\ell}}{(R_{i,\ell}^2 + h^2)^{\frac{b}{2}}} G_c(\phi_{i,\ell}) x_{i,\ell}. \quad (38)$$

This assumption is justified by the interfering ray-paths on every beamforming that have different attenuations and phase shifts, thus independent.  $\mathbf{w} = [w_1, w_2, \dots, w_L]^T$  is the collection of noise amplitudes. The LOS/NLOS links are shown in Fig. 10 and using the Weyl model (similar to Saleh-Valenzuela [46] adapted for mmW [47], [48]) where the indirect NLOS paths from the transmitter are reflected from a secondary point which is uniformly distributed around a circle with radius  $d$  around each of the transmitter's location. Usually, at high frequencies, there are not many NLOS paths so that typically are  $L = 2 - 3$  [49], [50], [51]. The receiver for  $L$  paths, possibly with different (and likely delay-resolvable for mmW and sub-THz system with large bandwidth) delays is expected to combine to maximize the service probability. If using the Maximal Ratio Combining (MRC) combiner for the  $L$  paths related to the user of interest affected by the interference powers  $I_\ell = |\iota_\ell|^2$ , one gets the following service probability analysis (see Appendix B for derivation and specific MRC notation):

$$P_{MRC} = \mathbb{P}_I \left( \sum_{\ell=1}^L \alpha_\ell I_\ell < \frac{1}{T} \left( \sum_{\ell=1}^L \frac{|\beta_\ell|^2}{\bar{I}_\ell^2 D_\ell^{2b}} \right)^2 \right). \quad (39)$$

where  $|\beta_\ell|^2$  is the fluctuation for the signal from the user of interest from  $\ell$ th path, and the distribution of total interference  $I_{MRC} = \sum_{\ell=1}^L \alpha_\ell I_\ell$  follows from the CF for iid interferers over the L-beamformers:

$$\Psi_{I_{MRC}}(\omega) = \prod_{\ell=1}^L \Psi_I(a_\ell \omega). \quad (40)$$

The NLOS distances  $D_\ell = (R_{o,\ell}^2 + h^2)^{1/2}$ , and  $R_{o,\ell}$  for  $\ell > 1$  are affected by the random angular position  $\eta$  of the NLOS reflections around the radius  $d$  as depicted in Fig. 10:

$$R_{o,\ell} = d + \sqrt{R_{o,1}^2 + d^2 - 2 d R_{o,1} \cos(\eta)} \quad \forall \ell > 1. \quad (41)$$

Pragmatically, NLOS distance for the served user is dependent on the specific multipath model assumed here, and a convenient way to incorporate the NLOS attenuation from the

additional path  $R_{o,\ell} - R_{o,1}$  is to approximate this term is by considering the mean distance for NLOS  $\bar{R}_{o,\ell} = E_{\eta}[R_{o,\ell}]$ . The distance  $\bar{D}_{\ell} = (\bar{R}_{o,\ell}^2 + h^2)^{1/2}$  is for the NLOS  $\ell > 1$  and thus the relationship (39) is somewhat simplified by constant distances. Recalling that LOS/NLOS models hold for interferers'  $i_{\ell}$ ; the power is augmented by the NLOS components, and service probability is reduced accordingly compared to  $L = 1$  (LOS-only). The CF for  $L > 1$  is derived in Appendix C, accounting for LOS and NLOS.

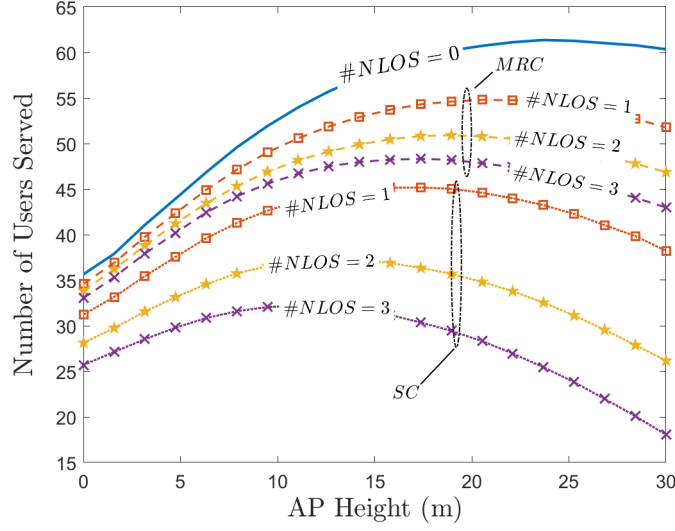


Figure 11. Average users served  $M_s$  within square area  $200\text{ m} \times 200\text{ m}$  vs. UCA height  $h$ , solid lines is the no NLOS ( $L = 1$ ), while dashed lines with marker are with NLOS for  $L = 2, 3, 4$ , with maximal ratio combining (MRC) and selection combining (SC) receivers for  $N_c = 500$ ,  $\lambda = 10^{-2}\text{ m}^{-2}$ ,  $2b = 2.6$ ,  $[T]_{dB} = 0$ ,  $|\beta_{\ell}|^2 = 1$  for every path  $\ell$

Fig. 11 and Fig. 12 show the average number of users served  $M_s$  within a  $\Delta \times \Delta$  square-shaped area (from (27) it is  $M_s = \lambda \Delta^2 \bar{P}_s$ ) when the AP with UCA is located at the center. The multipath increase the interference and increasing the number of NLOS paths from 1 to 3 (or  $L = 1, 2, 3, 4$ ). In Fig. 11 the performance degrades as the density of the interferers are quite high (here  $\lambda = 10^{-2}\text{ m}^{-2}$ ), but differently in Fig. 12 the aggregated interference is lower due to the lower density ( $\lambda = 10^{-3}\text{ m}^{-2}$ ) and thus there is a clear benefit arising from the multipath that vanishes for large height (here  $h > 25\text{ m}$ ). The performance from MRC received in Fig. 11 and Fig. 12 is compared to the selection combining (SC) that select the path with the largest SIR [52, Ch. 7]. Derivation of SC is straightforward (not shown here). As expected, the MRC outperforms the SC, but one might notice that degradation becomes more severe for large multipath. In the remainder of the paper, we consider the multipath condition with both LOS and NLOS links.

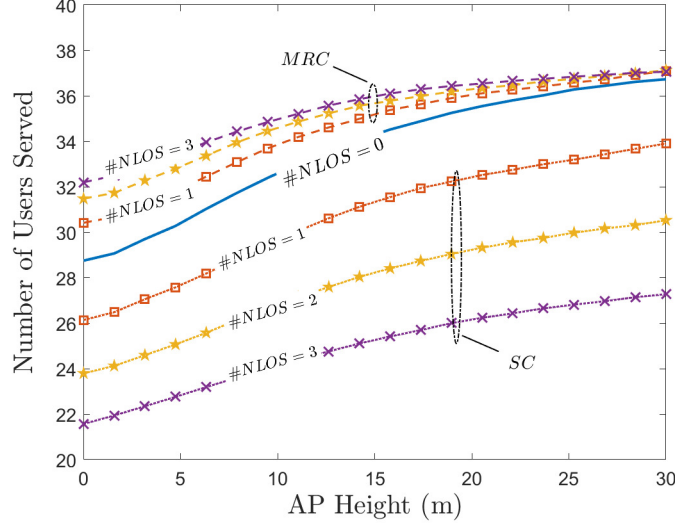


Figure 12. Average users served  $M_s$  within square area  $200\text{ m} \times 200\text{ m}$  vs. UCA height  $h$ , solid lines is the no NLOS ( $L = 1$ ), while dashed lines with marker are with NLOS for  $L = 2, 3, 4$ , with MRC and SC receivers for  $N_c = 500, \lambda = 10^{-3}\text{ m}^{-2}$ ;  $2b = 2.6$ ,  $[T]_{dB} = 0$ ,  $|\beta_\ell|^2 = 1$  for every path  $\ell$

### C. Noise

Even if the paper analyzes the aggregated interference power, in a 6G network with high path-loss it is inevitable to consider also the effect of the noise power. To take the noise power account, it is easy to prove that relation (39) must be modified:

$$\mathbb{P}_{service} = \mathbb{P}_I \left( I_{tot} + N_{tot} < \frac{1}{T} \left( \sum_{\ell=1}^L \frac{|\beta_\ell|^2}{\bar{I}_\ell D_\ell^{2b}} \right)^2 \right), \quad (42)$$

where  $I_{tot} = \sum_{\ell=1}^L \alpha_\ell I_\ell$  and  $N_{tot} = \sigma_n^2 \sum_{\ell=1}^L \alpha_\ell$  are the total interference power and noise power respectively, after MRC at the AP with  $\alpha_\ell = |\beta_\ell|^2 / (\bar{I}_\ell + \sigma_n^2) D_\ell^{2b}$ .

### D. Blockage

In mmW and 6G sub-THz systems the waves are prone to blockage due to static and dynamic blockage. Static blockage [53]–[55] is caused by structures like buildings, trees, etc., self-blockage [55]–[57] is caused by the body holding the UE, and dynamic blockage [55] is caused by moving objects, humans or vehicles. The behavior of blockages and their impact on the coverage probability and system performance are different. Some of the blockage effects can be modeled in closed form, while some others need numerical methods. Here we limit the analysis of the paper to the numerical evaluation of the coverage probability in the presence of blockage.



It is convenient to define a dummy binary variable  $\mu_\ell$  for the  $\ell$ -th path, which is  $\mu_\ell = 0$  when the link is blocked and  $\mu_\ell = 1$  when the link is free of any blockage, such that  $Prob(\mu_\ell = 0) = P_B$  is invariant on every path, and  $P_B$  is the probability of blockage. The blockage per path can be incorporated into (42) as

$$\mathbb{P}_{service} = \mathbb{P}_I \left( \tilde{I}_{tot} + \tilde{N}_{tot} < \frac{1}{T} \left( \sum_{\ell=1}^L \frac{|\beta_\ell|^2 \mu_\ell}{\bar{I}_\ell D_\ell^{2b}} \right)^2 \right), \quad (43)$$

where  $\tilde{I}_{tot} = \sum_{\ell=1}^L \tilde{\alpha}_\ell I_\ell \mu_\ell$  and  $\tilde{N}_{tot} = \sigma_n^2 \sum_{\ell=1}^L \tilde{\alpha}_\ell$  are the total interference and noise power respectively after MRC at the AP, with  $\tilde{\alpha}_\ell = \mu_\ell \alpha_\ell$  being a scaling parameter for a given path, and it is obviously switched off by  $\mu_\ell$  when the path is blocked.

The goal is to assess the effect of the impact of blockage  $P_B$  on service probability. At each snapshot, one link can be either blocked or available. In order to calculate the service probability, taking into account the blockage probability, one must numerically evaluate (43), for  $Prob(\mu_\ell = 0) = P_B$  for  $\forall \ell$ . Fig. 13 is the average service probability and Fig. 14

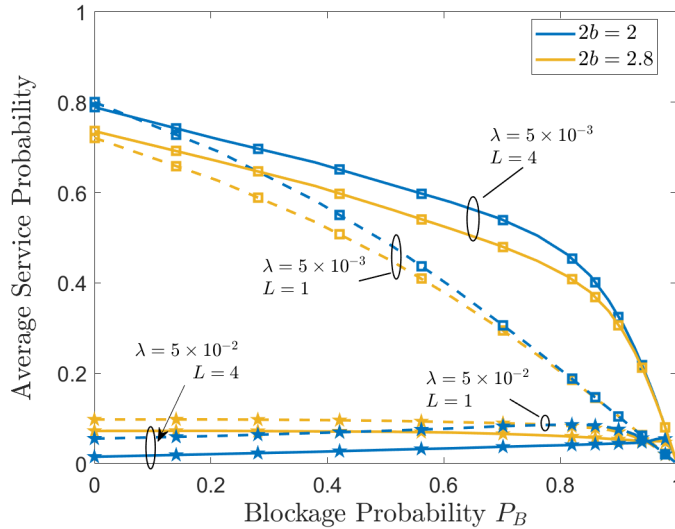


Figure 13. Average service probability vs the probability of blockage of all the links, for  $\lambda = \{5 \times 10^{-3}, 5 \times 10^{-2}\} m^{-2}$ , and number of paths  $L = \{1, 4\}$  where  $L = 1$  means that only LOS link exists. Parameters:  $P_{tx} = 20$  dB,  $NF = 7$  dB,  $BW = 400$  MHz,  $F_c = 28$  GHz, service area =  $100m \times 100m$  square, AP height  $h = 10$  m, threshold  $[T]_{dB} = 0$ .

is the number of UEs served, both figures are versus blockage probability  $P_B$  for small ( $\lambda = 5 \times 10^{-3} m^{-2}$ ) and large ( $\lambda = 5 \times 10^{-2} m^{-2}$ ) UEs density, and varying number of paths ( $L = 1, 4$ ), and path loss ( $2b = 2, 2.8$ ). On Fig. 13, for small  $\lambda$  and LOS path ( $L = 1$ ) the blockage probability makes the the service probability drop, while for  $L = 4$  the service probability is more robust even for large  $P_B$ , and this is due to the diversity of the multipath

against the interference. On the other hand, when  $\lambda = 5 \times 10^{-2} m^{-2}$  a multipath channel with  $L = 4$  degrades severely the performance. Numerical analysis shows the impact of the blockage on the service probability in Fig.13, and the average number of user served in Fig. 14. The total number of users within a  $\Delta \times \Delta$  square-shaped area is  $M_s = \lambda \Delta^2 \bar{P}_s$ . This means that for small  $P_B$  any increase of one decade of UE density makes a smaller variation in the number of users served. Recall that the number of UEs served in Fig. 14 refers to the UEs allocated in the same spectrum, and thus knowing the average number of UEs assignable on the same spectrum region, one can pre-design the largest number of users that a resource scheduler can expect to assign (not covered in this paper).

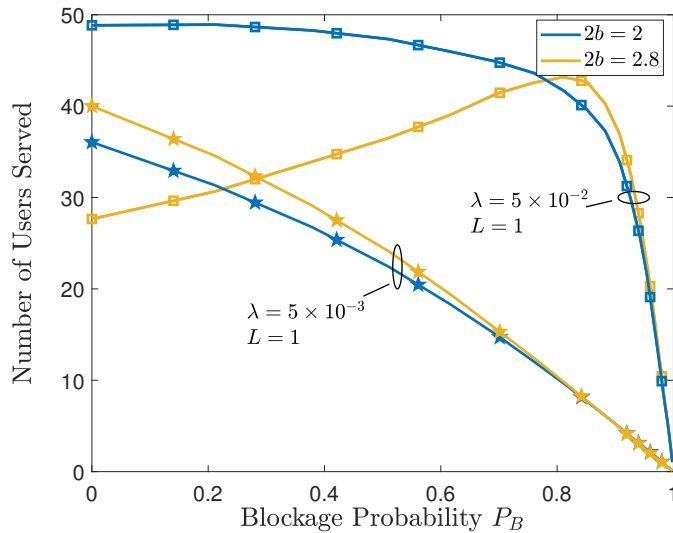


Figure 14. Average service probability vs the probability or blockage of all the links, for  $\lambda = \{5 \times 10^{-3}, 5 \times 10^{-2}\} m^{-2}$ , and number of paths  $L = \{1, 4\}$  where  $L = 1$  means that only LOS link exists. Parameters:  $P_{tx} = 20$  dB,  $NF = 7$ dB,  $BW = 400$  MHz,  $F_c = 28$  GHz, service area =  $100m \times 100m$  square, AP height  $h = 10m$ , threshold  $[T]_{dB} = 0$ .

## VI. CONCLUSIONS

In this paper, we derived tractable expressions for the characteristic function of the aggregate interference power for homogeneous distribution of UEs using the SG framework for  $N_c \times N_v$  UcyIA placed at arbitrary height. We proved that for  $h > 0$ , the distribution of the aggregated interference could be analytically approximated by a decomposable mixture of two distributions: skewed alpha-stable and Gaussian. The numerical analysis validates the results derived for the array configurations, including the case when  $N_v = 1$  for UCA. The analysis of average service probability vs. UcyIA height shows that there are different trade-offs to exploit. Furthermore, the appropriate array geometry depends on different environment

and propagation parameters. The impact of multipath has been evaluated analytically, thus, showing the trade-off by the increased aggregated interference, and the diversity for the UE of interest. Blockage makes the analysis to be very realistic for mmW and 6G system, and the blockage analysis has showed that there are several design insights to exploit.

Future work could consider the extension to distributed antenna systems (DAS) with different multi-AP coordination. The availability of the aggregated interference distributions in analytic form opens the possibility to explore multi-AP cooperation that are possible otherwise by massive simulations.

## APPENDIX

### APPENDIX A

#### SINGULARITY POINT

According to [58, sections 313.14 & 021.12] we have  $\int_0^\infty (e^{j\mu t})t^{-\alpha-1}dt = (-j\mu)^\alpha\Gamma(-\alpha)$  which is used in Ref. [9] when  $h = 0$  for proving the alpha-stability of the distribution of aggregated interference power. However, for  $h > 0$  one will encounter the following integral and its solution:

$$\int_0^{|\omega|/h^{2b}} \left[ \frac{1 - e^{j\mu t}}{t^{\alpha+1}} \right] dt = \lim_{\varepsilon \rightarrow 0} \left( (-j\mu)^\alpha \Gamma(-\alpha, -j\mu t) - \frac{1}{\alpha t^\alpha} \right) \Big|_{t=\varepsilon}^{t=|\omega|/h^{2b}}, \quad (44)$$

for any constant and real  $\mu$  and  $0 < \alpha < 1$ . In order to inspect the existence of any singularity point, one could use the series of incomplete Gamma function

$$\Gamma(x, z) = \Gamma(x) - z^x \sum_{k=0}^{\infty} \frac{(-z)^k}{(x+k)k!}. \quad (45)$$

Since  $x = -\alpha \in (-1, 0)$ , there exist one singularity point for  $z \rightarrow 0$  ( $t \rightarrow 0$  in (44)) that is compensated by the integral  $\int_0^{|\omega|/h^{2b}} \left[ \frac{1}{t^{\alpha+1}} \right] dt$ .

### APPENDIX B

#### PROOF OF MRC

Let the combiner be

$$\hat{x} = \sum_{\ell=1}^L c_\ell^H y_\ell = \mathbf{c}^H \mathbf{y}, \quad (46)$$

with weights  $\mathbf{c}$  from a received signal  $\mathbf{y} = \mathbf{h}\mathbf{x} + \boldsymbol{\nu}$  where the  $j$ th entry of  $\mathbf{h}$  is  $h_j = \beta_j/r_j^b$  for distance  $r_j$ , and the CF of the interference  $I_j = |\nu_j|^2$  is known  $\Psi_\ell(\omega)$ . The MRC are designed to maximize the SIR  $\Upsilon$ , and thus the service probability  $P_{MRC}(\mathbf{c})$  where the instantaneous SIR is

$$\Upsilon = \frac{\mathbf{c}^H \mathbf{h} \mathbf{h}^H \mathbf{c}}{\mathbf{c}^H \bar{\mathbf{D}}_I \mathbf{c}}, \quad (47)$$

$\bar{D}_I = E_I[D_I]$  for  $D_I = \text{diag}(I_1, I_2, \dots, I_L)$ , and  $\bar{I}_\ell = E[I_\ell]$  that can be derived from CF, such as for  $R_{max} < \infty$ . However, for skewed alpha-stable distributions for  $R_{max} \rightarrow \infty$  (UCA for  $h = 0$ , Sect.III-B), the mean does not exist, and maximization for the choice  $\bar{I}_\ell$  as median does not change the conclusions. The Rayleigh quotient (47) is known to be maximized for the choice

$$\mathbf{c}_{opt} = \frac{\bar{\mathbf{D}}_I^{-1} \mathbf{h}}{\mathbf{h}^H \bar{\mathbf{D}}_I^{-1} \mathbf{h}} \quad (48)$$

of the weights  $\mathbf{c}$ . The service probability reduces to

$$P_{MRC} = \mathbb{P}_I(\mathbf{c}_{opt}^H \mathbf{D}_I \mathbf{c}_{opt} < \mathbf{c}_{opt}^H \mathbf{h} \mathbf{h}^H \mathbf{c}_{opt} \frac{\sigma}{T}), \quad (49)$$

and after some analytic it reduces to

$$P_{MRC} = \mathbb{P}_I \left( I_{tot} < \frac{B}{T} \right), \quad (50)$$

where the aggregated weighted interference is  $I_{tot} = \sum_{\ell=1}^L I_\ell \alpha_\ell$  for  $\alpha_\ell = |\beta_\ell|^2 / (\bar{I}_\ell r_\ell^{2b})$  and  $B = \left( \sum_{\ell=1}^L |\beta_\ell|^2 / \bar{I}_\ell r_\ell^{2b} \right)^2$ . Thus, the analysis for the service (or complementary, for the outage) depends on the CDF of  $I_{tot}$  and in turn on the CF

$$\Psi_{I_{tot}}(\omega) = \prod_{\ell=1}^L \Psi_\ell(a_\ell \omega). \quad (51)$$

that evidences the multiple usage in the main text for service probability analysis.

## APPENDIX C

### AUGMENTED INTERFERENCE

By considering the geometric model used for the NLOS paths, the CF of the aggregated interference power for an isotropic antenna (can be readily generalized for UCA or UcyIA but it is avoided here for simplicity) by re-adapting relation (24) with small approximations, for NLOS paths calculated as  $\Psi_{NLOS}(\omega) = \Psi_1(\omega) \cdot \Psi_2(\omega)$ , where

$$\begin{aligned} \Psi_1(\omega) &= \exp \left( -\frac{\pi\lambda}{C_\alpha} |\omega|^\alpha |\bar{\beta}|^{2\alpha} P \left( -\alpha, \frac{-j|\omega|\bar{\beta}^2}{(h^2 + d^2)^b} \right) \left( 1 - j \text{sign}(\omega) \tan \frac{\pi\alpha}{2} \right) + \pi\lambda(h^2 + d^2) \right), \\ \Psi_2(\omega) &= \exp \left( +\frac{\pi\lambda d}{C_\alpha} |\omega|^{\frac{\alpha}{2}} |\bar{\beta}|^{2\alpha} P \left( \frac{-\alpha}{2}, \frac{-j|\omega|\bar{\beta}^2}{(h^2 + d^2)^b} \right) \left( 1 - j \text{sign}(\omega) \tan \frac{\pi\alpha}{4} \right) + 2\pi\lambda d \sqrt{h^2 + d^2} \right). \end{aligned}$$

Now, the CF of the total augmented aggregate interference is

$$\Psi_I(\omega) = \Psi_{NLOS}^{(L-1)}(\omega) \Psi_{LOS}(\omega) \quad (52)$$

where  $\Psi_{LOS}(\omega)$  is as derived as in relation (24) and  $L$  is the total number of paths. The CDF of the augmented interference can be achieved from this CF.

## REFERENCES

- [1] N. Panwar, S. Sharma, and A. K. Singh, "A survey on 5g: The next generation of mobile communication," *Physical Communication*, vol. 18, pp. 64–84, 2016, special Issue on Radio Access Network Architectures and Resource Management for 5G. [Online]. Available: <https://www.sciencedirect.com/science/article/pii/S1874490715000531>
- [2] T. T. S. Rappaport, S. Sun, R. Mayzus, H. Zhao, Y. Azar, K. Wang, G. N. Wong, J. K. Schulz, M. Samimi, and F. Gutierrez, "Millimeter wave mobile communications for 5g cellular: It will work!" *IEEE Access*, vol. 1, pp. 335–349, 2013.
- [3] F. Qamar, M. U. A. Siddiqui, M. N. Hindia, R. Hassan, and Q. N. Nguyen, "Issues, challenges, and research trends in spectrum management: A comprehensive overview and new vision for designing 6g networks," *Electronics*, vol. 9, no. 9, 2020. [Online]. Available: <https://www.mdpi.com/2079-9292/9/9/1416>
- [4] L. Azpilicueta, P. Lopez, J. Zuniga-Mejia, M. Celaya, F. A. Rodr guez, C. Vargas, E. Aguirre, D. G. Michelson, and F. Falcone, "Fifth-generation (5g) mmwave spatial channel characterization for urban environments system analysis," *Sensors*, vol. 20, no. 18, 2020.
- [5] M. Ikram, K. Sultan, M. F. Lateef, and A. S. M. Alqadami, "A road towards 6g communication;a review of 5g antennas, arrays, and wearable devices," *Electronics*, vol. 11, no. 1, 2022. [Online]. Available: <https://www.mdpi.com/2079-9292/11/1/169>
- [6] R. Singh, W. Lehr, D. Sicker, and K. Huq, "Beyond 5g: The role of thz spectrum," *SSRN Electronic Journal*, 01 2019.
- [7] K. Dong, M. Mizmizi, D. Tagliaferri, and U. Spagnolini, "Vehicular blockage modelling and performance analysis for mmwave v2v communications," 2021.
- [8] H. Q. Ngo, E. G. Larsson, and T. L. Marzetta, "Energy and spectral efficiency of very large multiuser mimo systems," *IEEE Transactions on Communications*, vol. 61, no. 4, pp. 1436–1449, 2013.
- [9] M. Z. Win, P. C. Pinto, and L. A. Shepp, "A mathematical theory of network interference and its applications," *Proceedings of the IEEE*, vol. 97, no. 2, pp. 205–230, Feb 2009.
- [10] M. Baianifar, S. Khavari, S. M. Razavizadeh, and T. Svensson, "Impact of user height on the coverage of 3d beamforming-enabled massive mimo systems," in *2017 IEEE 28th Annual International Symposium on Personal, Indoor, and Mobile Radio Communications (PIMRC)*, Oct 2017, pp. 1–5.
- [11] A. Mouradian, "Modeling dense urban wireless networks with 3d stochastic geometry," *Performance Evaluation*, vol. 121–122, pp. 1 – 17, 2018. [Online]. Available: <http://www.sciencedirect.com/science/article/pii/S0166531617300287>
- [12] H. ElSawy, A. Sultan-Salem, M. Alouini, and M. Z. Win, "Modeling and analysis of cellular networks using stochastic geometry: A tutorial," *IEEE Communications Surveys Tutorials*, vol. 19, no. 1, pp. 167–203, Firstquarter 2017.
- [13] H. ElSawy, E. Hossain, and M. Haenggi, "Stochastic geometry for modeling, analysis, and design of multi-tier and cognitive cellular wireless networks: A survey," *IEEE Communications Surveys Tutorials*, vol. 15, no. 3, pp. 996–1019, Third 2013.
- [14] S. Weber and J. G. Andrews, "Transmission capacity of wireless networks," *CoRR*, vol. abs/1201.0662, 2012. [Online]. Available: <http://arxiv.org/abs/1201.0662>
- [15] T. Bai and R. W. Heath, "Analyzing uplink sinr and rate in massive mimo systems using stochastic geometry," *IEEE Transactions on Communications*, vol. 64, no. 11, pp. 4592–4606, Nov 2016.
- [16] M. D. Renzo, A. Guidotti, and G. E. Corazza, "Average rate of downlink heterogeneous cellular networks over generalized fading channels: A stochastic geometry approach," *IEEE Transactions on Communications*, vol. 61, no. 7, pp. 3050–3071, July 2013.
- [17] M. Filo, C. H. Foh, S. Vahid, and R. Tafazolli, "Performance impact of antenna height in ultra-dense cellular networks," in *2017 IEEE International Conference on Communications Workshops (ICC Workshops)*, 2017, pp. 429–434.
- [18] J. Liu, M. Sheng, K. Wang, and J. Li, "The impact of antenna height difference on the performance of downlink cellular networks," 2017.

- [19] A. Al-Hourani, S. Kandeepan, and S. Lardner, "Optimal lap altitude for maximum coverage," *IEEE Wireless Communications Letters*, vol. 3, no. 6, pp. 569–572, Dec 2014.
- [20] K. Yoshikawa, K. Yamamoto, T. Nishio, and M. Morikura, "Grid-based exclusive region design for 3d uav networks: A stochastic geometry approach," *IEEE Access*, vol. 7, pp. 103 806–103 814, 2019.
- [21] M. M. Azari, F. Rosas, A. Chiumento, and S. Pollin, "Coexistence of terrestrial and aerial users in cellular networks," in *2017 IEEE Globecom Workshops (GC Wkshps)*, Dec 2017, pp. 1–6.
- [22] E. Chu, J. M. Kim, and B. C. Jung, "Interference modeling and analysis in 3-dimensional directional uav networks based on stochastic geometry," *ICT Express*, 2019.
- [23] D. Maamari, N. Devroye, and D. Tuninetti, "Coverage in mmwave cellular networks with base station co-operation," *IEEE Transactions on Wireless Communications*, vol. 15, no. 4, pp. 2981–2994, April 2016.
- [24] M. Cheng, J. Wang, Y. Wu, X. Xia, K. Wong, and M. Lin, "Coverage analysis for millimeter wave cellular networks with imperfect beam alignment," *IEEE Transactions on Vehicular Technology*, vol. 67, no. 9, pp. 8302–8314, Sep. 2018.
- [25] J. G. Andrews, F. Baccelli, and R. K. Ganti, "A tractable approach to coverage and rate in cellular networks," *IEEE Transactions on Communications*, vol. 59, no. 11, pp. 3122–3134, November 2011.
- [26] T. Alwajeeh, P. Combeau, R. Vauzelle, and A. Bounceur, "A high-speed 2.5d ray-tracing propagation model for microcellular systems, application: Smart cities," in *2017 11th European Conference on Antennas and Propagation (EUCAP)*, 2017, pp. 3515–3519.
- [27] Z. Liu, L.-X. Guo, and W. Tao, "Full automatic preprocessing of digital map for 2.5d ray tracing propagation model in urban microcellular environment," *Waves in Random and Complex Media*, vol. 23, 08 2013.
- [28] X. Yu, J. Zhang, M. Haenggi, and K. B. Letaief, "Coverage analysis for millimeter wave networks: The impact of directional antenna arrays," *IEEE Journal on Selected Areas in Communications*, vol. 35, no. 7, pp. 1498–1512, July 2017.
- [29] L. Josefsson and P. Persson, *Conformal array antenna theory and design*. John Wiley & sons, 2006, vol. 29.
- [30] J. G. Andrews, T. Bai, M. N. Kulkarni, A. Alkhateeb, A. K. Gupta, and R. W. Heath, "Modeling and analyzing millimeter wave cellular systems," *IEEE Transactions on Communications*, vol. 65, no. 1, pp. 403–430, Jan 2017.
- [31] S. Stergiopoulos and A. C. Dhanantwari, "Implementation of adaptive processing in integrated active-passive sonars with multi-dimensional arrays," in *1998 IEEE Symposium on Advances in Digital Filtering and Signal Processing. Symposium Proceedings (Cat. No.98EX185)*, June 1998, pp. 62–66.
- [32] S. M. Razavizadeh, M. Ahn, and I. Lee, "Three-dimensional beamforming: A new enabling technology for 5g wireless networks," *IEEE Signal Processing Magazine*, vol. 31, no. 6, pp. 94–101, Nov 2014.
- [33] N. Wu, F. Zhu, and Q. Liang, "Evaluating spatial resolution and channel capacity of sparse cylindrical arrays for massive mimo," *IEEE Access*, vol. 5, pp. 23 994–24 003, 2017.
- [34] H. L. V. Trees, *Detection, Estimation, and Modulation Theory, Part III: Radar Sonar Signal Processing and Gaussian Signals in Noise*. John Wiley & Sons, INC., 2001.
- [35] U. Spagnolini, *Statistical Signal Processing in Engineering*. John Wiley & Sons, Incorporated, 2018. [Online]. Available: <https://books.google.it/books?id=yTg9swEACAAJ>
- [36] H. Shokri-Ghadikolaei and C. Fischione, "Millimeter wave ad hoc networks: Noise-limited or interference-limited?" in *2015 IEEE Globecom Workshops (GC Wkshps)*, 2015, pp. 1–7.
- [37] M. Wildemeersch, T. Q. S. Quek, M. Kountouris, A. Rabbachin, and C. H. Slump, "Successive interference cancellation in heterogeneous networks," *IEEE Transactions on Communications*, vol. 62, no. 12, pp. 4440–4453, Dec 2014.
- [38] A. Rabbachin, T. Q. S. Quek, H. Shin, and M. Z. Win, "Cognitive network interference," *IEEE Journal on Selected Areas in Communications*, vol. 29, no. 2, pp. 480–493, February 2011.

- [39] X. Chen, D. W. K. Ng, W. Yu, E. G. Larsson, N. Al-Dhahir, and R. Schober, "Massive access for 5g and beyond," 2020.
- [40] Y. Wen, S. Loyka, and A. Yongacoglu, "The impact of fading on the outage probability in cognitive radio networks," in *2010 IEEE 72nd Vehicular Technology Conference - Fall*, 2010, pp. 1–5.
- [41] J. Nolan, *Stable distributions: models for heavy-tailed data*. Birkhauser New York, 2003.
- [42] R. B. Davies, "Numerical inversion of a characteristic function," *Biometrika*, vol. 60, no. 2, pp. 415–417, 1973.
- [43] N. G. Shephard, "From characteristic function to distribution function: a simple framework for the theory," *Econometric theory*, vol. 7, no. 4, pp. 519–529, 1991.
- [44] M. A. T. Figueiredo and A. K. Jain, "Unsupervised learning of finite mixture models," *IEEE Transactions on Pattern Analysis and Machine Intelligence*, vol. 24, no. 3, pp. 381–396, 2002.
- [45] M. R. Akdeniz, Y. Liu, M. K. Samimi, S. Sun, S. Rangan, T. S. Rappaport, and E. Erkip, "Millimeter wave channel modeling and cellular capacity evaluation," *IEEE Journal on Selected Areas in Communications*, vol. 32, no. 6, pp. 1164–1179, 2014.
- [46] A. A. M. Saleh and R. Valenzuela, "A statistical model for indoor multipath propagation," *IEEE Journal on Selected Areas in Communications*, vol. 5, no. 2, pp. 128–137, 1987.
- [47] Z. Peize, "Radio propagation and wireless coverage of Isaa-based 5g millimeter-wave mobile communication systems," 06 2019.
- [48] M. Flament and A. Svensson, "Virtual cellular networks for 60 ghz wireless infrastructure," 06 2003, pp. 1223 – 1227 vol.2.
- [49] M. K. Samimi and T. S. Rappaport, "3-d millimeter-wave statistical channel model for 5g wireless system design," *IEEE Transactions on Microwave Theory and Techniques*, vol. 64, no. 7, pp. 2207–2225, 2016.
- [50] T. S. Rappaport, G. R. MacCartney, M. K. Samimi, and S. Sun, "Wideband millimeter-wave propagation measurements and channel models for future wireless communication system design," *IEEE Transactions on Communications*, vol. 63, no. 9, pp. 3029–3056, 2015.
- [51] M. R. Akdeniz, Y. Liu, M. K. Samimi, S. Sun, S. Rangan, T. S. Rappaport, and E. Erkip, "Millimeter wave channel modeling and cellular capacity evaluation," *IEEE Journal on Selected Areas in Communications*, vol. 32, no. 6, pp. 1164–1179, 2014.
- [52] A. Goldsmith, *Wireless Communications*. Cambridge University Press, 2005.
- [53] T. Bai, R. Vaze, and R. W. Heath, "Using random shape theory to model blockage in random cellular networks," in *2012 International Conference on Signal Processing and Communications (SPCOM)*, 2012, pp. 1–5.
- [54] —, "Analysis of blockage effects on urban cellular networks," *IEEE Transactions on Wireless Communications*, vol. 13, no. 9, pp. 5070–5083, 2014.
- [55] I. K. Jain, R. Kumar, and S. S. Panwar, "The impact of mobile blockers on millimeter wave cellular systems," *IEEE Journal on Selected Areas in Communications*, vol. 37, no. 4, pp. 854–868, 2019.
- [56] A. K. Gupta, J. G. Andrews, and R. W. Heath, "Macrodiversity in cellular networks with random blockages," *IEEE Transactions on Wireless Communications*, vol. 17, no. 2, pp. 996–1010, 2018.
- [57] K. Venugopal and R. W. Heath, "Millimeter wave networked wearables in dense indoor environments," *IEEE Access*, vol. 4, pp. 1205–1221, 2016.
- [58] W. G. Hofreiter, *Integraltafel*. Springer-Verlag Wien GMBH, 1950.